
Methods¹

Expedition 307 Scientists²

Chapter contents

Introduction	1
Lithostratigraphy	4
Biostratigraphy	7
Paleomagnetism	8
Geochemistry and microbiology	9
Physical properties	14
Downhole measurements	19
References	23
Figures	27
Tables	37

Introduction

Information assembled in this chapter will help the reader understand the basis for our preliminary conclusions and enable the interested investigator to select samples for further analysis. This information concerns only shipboard operations and analyses described in the site reports in the Expedition Reports section of the Expedition 307 *Proceedings of the Integrated Ocean Drilling Program* (IODP) volume. Methods used by various investigators for shore-based analyses of Expedition 307 samples will be described in the individual contributions published in the Research Results section of the Expedition 307 *Proceedings* volume and in publications in various professional journals.

Authorship of site chapters

The separate sections of the site chapters were written by the following shipboard scientists (listed in alphabetical order, no seniority is implied):

Expedition summary and principal results: Expedition 307 Scientists

Background and objectives: Timothy Ferdelman, Akihiro Kano
Operations: Derryl Schroeder, Trevor Williams

Lithostratigraphy: Miriam Andres, Morten Bjerager, Boris Dorschel, Jay Gregg, Xianghui Li, Ivana Novosel, Keiichi Sasaki, Chizuru Takashima, Jürgen Titschack

Biostratigraphy: Kohei Abe, Emily Browning

Paleomagnetism: Anneleen Foubert, Yuji Fuwa

Geochemistry and microbiology: Barry Cragg, Tracy Frank, Jim Gharib, Philippe Léonide, Kai Mangelsdorf, Saburo Sakai, Vladimir Samarkin, Arthur Spivack

Physical properties and stratigraphic correlation: Veerle Huvenne, Ben De Mol, Xavier Monteys, Akiko Tanaka

Downhole logging: Philippe Gaillot

Drilling operations

Three standard coring systems were used during Expedition 307: the advanced piston corer (APC), the extended core barrel (XCB), and the rotary core barrel (RCB). These standard coring systems and their characteristics are summarized in the “Methods” chapters of previous *Proceedings* volumes as well a number of Ocean Drilling Program (ODP) *Technical Notes*. Most cored intervals were ~9.5 m long, which is the length of a standard core barrel. In

¹Expedition 307 Scientists, 2006. Methods. In Ferdelman, T.G., Kano, A., Williams, T., Henriot, J.-P., and the Expedition 307 Scientists. *Proc. IODP, 307*: Washington, DC (Integrated Ocean Drilling Program Management International, Inc.). doi:10.2204/iodp.proc.307.102.2006

²Expedition 307 Scientists' addresses.



some cases, the drill string was drilled, or “washed ahead,” without recovering sediments to advance the drill bit to a target depth where core recovery needed to resume.

Drilled intervals are referred to in meters below rig floor (mbrf), which are measured from the kelly bushing on the rig floor to the bottom of the drill pipe, and meters below seafloor (mbsf), which are calculated from the length of pipe deployed less estimated seafloor depth. When sediments of substantial thickness cover the seafloor, the mbrf depth of the seafloor is determined with a mudline core, assuming 100% recovery for the cored interval in the first core. Water depth is calculated by subtracting the distance from the rig floor to sea level from the mudline measurement in mbrf. This water depth usually differs from precision depth recorder measurements by a few meters, though the difference can be larger in areas of steep seafloor slopes. The mbsf depths of core tops are determined by subtracting the seafloor depth (mbrf) from the core-top depth (mbrf). The resulting core-top datums in mbsf are the ultimate reference for any further depth calculation procedures.

Drilling deformation

When cores are split, many show signs of significant sediment disturbance, including the concave-downward appearance of originally horizontal bedding, haphazard mixing of lumps of different lithologies (mainly at the tops of cores), fluidization, and flow-in. The latter three disturbances can be particularly severe during XCB and RCB drilling. Core deformation may also occur during retrieval because of changes in pressure and temperature as the core is raised and during cutting and core handling on deck.

Curatorial procedures and sample depth calculations

Numbering of sites, holes, cores, and samples follows standard IODP procedure. A full curatorial identifier for a sample consists of the expedition, site, hole, core number, core type, section number, and interval in centimeters measured from the top of the core section. For example, a sample identification of 307-U1316A-1H-1, 10–12 cm, represents a sample removed from the interval between 10 and 12 cm below the top of Section 1, Core 1 (H designates that this core was taken with the APC) of Hole U1316A during Expedition 307. Cored intervals are also referred to in “curatorial” mbsf. The mbsf depth of a sample is calculated by adding the depth of the sample below the section top and the lengths of all

higher sections in the core to the core-top datum measured with the drill string.

A sediment core from less than a few hundred mbsf may, in some cases, expand upon recovery (typically 10% in the uppermost 300 mbsf), and its length may not necessarily match the drilled interval. In addition, a coring gap is typically present between cores. Thus, a discrepancy may exist between the drilling mbsf and the curatorial mbsf. For instance, the curatorial mbsf of a sample taken from the bottom of a core may be larger than that of a sample from the top of the subsequent core, where the latter corresponds to the drilled core-top datum.

If a core has incomplete recovery, all cored material is assumed to originate from the top of the drilled interval as a continuous section for curation purposes. The true depth interval within the cored interval is not known. This should be considered as a sampling uncertainty in age-depth analysis and correlation of core facies with downhole log signals. See the discussions in [“Downhole measurements”](#) and [“Physical properties”](#) on the prospects for correlation of the curatorial depths (mbsf) or meters composite depths (mcd) with logging information to obtain a “true” depth interval.

Core handling and analysis

The original drilling strategy of Expedition 307 was to first drill Hole A using APC and XCB drilling for stratigraphy and develop a coarse geochemical framework (sulfate and methane) for making drilling decisions on holes assigned for microbiological sampling. After downhole logging of Hole A, Hole B would be dedicated to high-resolution microbiological and geochemical sampling and drilled to depth of APC refusal. Hole C would be drilled by RCB and dedicated to high-resolution stratigraphy, filling any coring gaps identified by stratigraphic correlation of the first two holes (see [“Composite section development”](#)) and extending the microbiology and geochemical sampling studies. However, after Site U1316, drilling contingencies forced us to alter our plan. For Site U1317, microbiological and geochemical sampling proceeded first and at relatively high resolution in Hole U1317A. Although sections for microbiological analysis were missing, opening cores from Hole U1317A allowed the sedimentologists to gather immediate information concerning the mound facies. This critical information further led to our decision to freeze and saw coral-bearing sections from subsequent holes (see [“Frozen cores”](#)).

Drilling during Expedition 307 entailed two changes to the normal core flow in the laboratories. First, the presence of coral, coral rubble, and dropstones

meant that cores could not be split using the normal core cutting techniques employed for nonlithified sediments. Second, a strong microbiological and geochemical component of Expedition 307 necessitated the adoption of a core flow scheme to deal with sensitive microbiological samples. Upon arrival on the catwalk, routine shipboard safety and pollution prevention samples along with acridine orange direct count (AODC) syringe samples and methane gas samples were collected (see “[Geochemistry and microbiology](#)”). A sample was removed from the core catcher and taken to the micropaleontology laboratory for rapid biostratigraphic determination. When the core was cut into sections, whole-round samples were taken for shipboard interstitial water examinations. On nonmicrobiological core sections, whole cores were run through a “Fast Track” multisensor core logger (MSCL) equipped with two magnetic susceptibility loops to facilitate real-time drilling decisions concerning the presence of corals and to maximize stratigraphic overlap between holes (see “[Composite section development](#)”). Whole-round core sections were then run through the multisensor track (MST), and thermal conductivity measurements were taken. At Site U1317, the presence of corals meant that a large fraction of cores were not split on board (see “[Frozen cores](#)”). Because these sediments were likely to contain magnetic sulfide minerals that can rapidly decompose in air, cores were measured on the cryogenic magnetometer as whole rounds.

The working half of each core was sampled for basic shipboard analysis (i.e., physical properties, carbonate, and bulk X-ray diffraction mineralogy) and for ephemeral minerals such as greigite for shore-based studies. In general, however, shipboard sampling was kept to a minimum during Expedition 307 to wait for opening and description at the IODP Bremen Core Repository (BCR). When short pieces of sedimentary rock were recovered, the individual pieces were split with the rock saw and placed in split liner compartments created by sealing spacers into the liners with acetone.

The archive-half sections were scanned on the digital imaging system, measured for color reflectance on the archive multisensor track (AMST), described visually and by means of smear slides, run through the cryogenic magnetometer, and finally photographed with color film one whole core at a time. Digital close-up photographs were taken of particular features for illustrations in site summary reports, as requested by scientists. Both halves of the core were then put into labeled plastic tubes, sealed, and transferred to cold storage space aboard the ship. At the end of the expedition in Mobile, Alabama (USA), the

cores were transferred to the IODP Gulf Coast Core Repository (GCR) and then on to BCR, where core description and sampling parties took place in October 2005.

Frozen cores

Coral-bearing cores pose problems for conventional core splitting in that the wire drags coral pieces up the core face or breaks them into fragments. Sawing unfrozen cores produced a surface layer of grime, coral fragments, and matrix that could not be scraped off without damaging the sedimentary structures. Depending on the coral preservation, freezing the cores before splitting results in undamaged split cores with a clean split-core face (this method had been successful for short cores from a nearby location collected by the *Marion Dufresne*). Approximately 67 cores were coral-bearing and thus suitable for frozen splitting (Site U1317, 0–155 mbsf; Site U1316, 50–55 mbsf):

- Cores from Hole U1317A were split conventionally with the saw to establish lithostratigraphy and coral content and to check the state of the split core face.
- Core U1316B-6H was the first test of the freeze and split procedure.
- Cores U1317C-1H through 6H were frozen and split during the expedition.
- Cores U1317C-7H through 16H were frozen and split during the transit from Ponta Delgada, Azores (Portugal), to Mobile.
- Cores from Holes U1317B and U1317E were frozen and split at GCR in August 2005.

The procedure for frozen-core splitting is as follows. A core patch is placed around the liner because the butyrate liner becomes brittle and fragile after freezing. The cores are frozen at between -20° and -50°C . The temperature range of the onboard freezers was between -50° and -86°C . A balance has to be struck: too warm and the core starts to melt during splitting, too cold and the butyrate liner becomes more brittle and the risk of sediment damage increases. The cores were split with a saw and transferred to new liners while frozen, in which state the cores can generally be lifted without breaking. The cores were warmed to about -10°C in the walk-in freezer, and the core surface was scraped clear of grime.

Some adjustments to conventional core flow were required. Cores frozen and split on board had to be cut into 1.2 m lengths in order to fit into the upright freezer and were run through the MST and cryogenic magnetometer (see “[Paleomagnetism](#)”) before freezing. Cores reentered the core flow after splitting and

out of sequence because of the >24 h freezing and splitting process. Cores left unopened on board for freezing and splitting at GCR were cut into conventional 1.5 m lengths and measured on the shipboard MST and cryogenic magnetometer. Minimum required measurements (core photos, color reflectance, and lithological description) were done postcruise.

Microbiological sampling

Two additional objectives of sampling during Expedition 307 were to obtain (1) high-resolution interstitial water geochemical profiles to delineate microbial reaction zones and evaluate potential zones of hydrocarbon flow and (2) corresponding samples for a variety of microbiological and biogeochemical analyses to be performed primarily in shore-based laboratories. Since microorganisms existing at deepwater seafloor temperatures (2°–4°C) can be acutely sensitive to elevated temperature (>10°C) and oxygen, we recognized a critical need to prevent thermal equilibration and exposure of the cores to oxygen after recovery. Sampling strategies, core flow, and subsampling for shore-based laboratories generally followed a modified scheme developed during Ocean Drilling Program (ODP) Leg 201. To minimize equilibration of the cores, the core barrel was extracted from the drill string and immediately transferred to the catwalk and marked by the IODP curatorial staff into 1.5 m sections. Shipboard microbiologists identified one or more 1.5 m sections (hereafter referred to as the MBIO sections) for rapid microbiological processing. Once the MBIO sections were selected, they were labeled with a red permanent marker with orientation and section number and removed from the core. Ends of the removed sections were covered with plastic caps but not sealed, and the sections were carried into the hold refrigerator, which was set to ~4°C and served as a microbiology cold room. Multiple sections were moved to the cold room to ensure that sufficient undisturbed material was available for microbiology and geochemistry sampling. At Site U1318, the sections identified for microbiology were first run through the Fast Track MSCL (a 5–10 min delay). Because of the short duration of scientific operations, the primary emphasis was on cleanly cutting and properly sampling the requisite number of whole-round cores for shore-based experimentation and analysis, as described in **“Whole-round core sampling in the cold room.”** Unsampled microbiological subsections and the remainder of the core on the catwalk were processed as described above. Frozen and cooled microbiology and geochemistry samples were shipped to shore-based laboratories from Ponta Delgada.

Lithostratigraphy

Sediment classifications

Sediments were classified based on their grain-size, composition, macrofossil content, and texture.

Mineralogy

Three sediment types were defined based on the following mineralogy: (1) carbonate-dominated sediments, (2) siliciclastic-dominated sediments, and (3) marine noncarbonate minerals. Their definitions are as follows.

Carbonate-dominated sediments are coarse- to fine-grained particles that consist of calcareous skeletal and nonskeletal grains and fragments (e.g., bioclasts and micrite). The term “micrite” is used to define very fine calcareous particles (<20 µm) of indeterminate origin. Carbonate sediments were classified after the modified Dunham classification from Embry and Klovan (1971). Dominating components were added as a prefix to the name (e.g., coral floatstone).

Siliciclastic grains were defined as (1) grains comprising minerals and rock fragments eroded from plutonic, sedimentary, and metamorphic strata and (2) grains comprising glass shards, rock fragments, and minerals produced by volcanic processes.

Marine noncarbonate minerals were (1) glauconite, a black to greenish, iron-rich sheet silicate that occurs as infill and rounded sand-sized grains; (2) phosphorides, commonly black sand- to gravel-sized grains; (3) framboidal pyrite; (4) barite; and (5) dolomite, which occurs as scattered rhombs.

Carbonate sediments

Carbonates were defined as sediments containing >50% carbonate, whereas siliciclastic sediments were defined as containing >50% siliciclastic grains.

Texture

The texture of calcareous sediments was classified after Dunham (1962) in conjunction with depositional textures described by Embry and Klovan (1971) (Fig. F1). Accordingly, carbonate crystals or fragments that are <20 µm are referred to as micrite. Within the coarse-grained carbonates (i.e., from floatstone to boundstone), the matrix between bioclasts ranges from mudstone to grainstone.

Siliciclastic sediments

Texture, structure, and composition are the main criteria for the selection of a principal name for siliciclastic sediments. The Udden-Wentworth grain-size

scale (Wentworth, 1922) (Fig. F2) defines the grain-size ranges and names of the textural groups (gravel, sand, silt, and clay) and subgroups (fine sand, coarse silt, etc.). When two or more textural groups or subgroups are present, the principal names appear in order of increasing abundance. Eight major textural categories can be defined on the basis of the relative proportions of sand, silt, and clay (Fig. F3). The terms “conglomerate” and “breccia” are the principal names of gravels with well rounded and angular clasts, respectively.

Major and minor modifiers

The lithologic classification of granular sediments was refined by adding major and minor modifiers (Table T1). Minor modifiers are preceded by the term “with.” The most common uses of major and minor modifiers are to describe the composition and textures of grain types that are present in major (25%–40%) and minor (10%–25%) proportions. In addition, major modifiers can be used to describe grain fabric, grain shape, and sediment color.

The composition of grains can be described in greater detail with the major and minor modifiers “coral,” “foraminifer,” “calcareous,” and “siliceous.” The terms calcareous and siliceous are used to describe sediments that are composed of calcareous or siliceous pelagic grains of uncertain origin.

The compositional terms for calcareous grains include the following major and minor modifiers as skeletal and nonskeletal grains:

- Bioclast = fragments of skeletal remains (specific names such as “molluscan” or “gastropodan” are used where appropriate).
- Pellet = fecal particles from deposit-feeding organisms.
- Peloid = micritized carbonate particles of unknown origin.
- Intraclast = a reworked carbonate sediment/rock fragments or rip-up clasts consisting of the same lithology as the host sediment.
- Lithoclast = a reworked carbonate rock fragment consisting of a different lithology than the host sediment.
- Calcareous, dolomitic, aragonitic, and sideritic = the mineral composition of carbonate muds or mudstones (micrite) of neritic origin.

The textural designations for siliciclastic grains used standard major and minor modifiers such as gravel(ly), sand(y), silt(y), and clay(ey). The character of siliciclastic grains can be described further by mineralogy using modifiers such as “quartz,” “feldspar,” “glauconite,” “mica,” “lithic,” or “calcareous.” The fabric of a sediment can be described us-

ing major modifiers such as “grain-supported,” “matrix-supported,” and “imbricated.” Fabric terms are generally useful only when describing gravels, conglomerates, and breccias.

In lithologies where the dominant grain size was 20–63 μm and the sediments were well sorted with grains in contact with each other, we placed the major modifier “silt-sized” before the principal name (e.g., silt-sized grainstone), according to Dunham’s (1962) classification. Modifiers such as “fine sand-sized” are also used to refine the description of sand-sized grainstones in the Lithologic Description section on the barrel sheets.

Whenever dolomite or dolomitic texture was recognized (>25%) in carbonate sediments, the term “dolomitic” was used as a major modifier (e.g., dolomitic mudstone with clay). When a lithology appeared to contain more than ~75% dolomite, it was called “dolostone” or, if skeletal components can be recognized, “skeletal dolostone.”

Sediments were named on the basis of their texture and major and minor modifiers (Table T1). Principal names define the granular sediment class (Fig. F3). Composition is the most important classifier to distinguish calcareous and siliciclastic sediments. The texture is significant for the further classification of calcareous sediments (Fig. F1). Composition and texture of cored sediments were determined aboard ship by visual observation as well as smear slides, thin sections, and coarse fractions. Calcium carbonate content was qualitatively estimated in smear slides and quantitatively estimated by coulometric analysis (see “Geochemistry and microbiology”).

Lithification

Lithification of recovered materials was defined according to Gealy et al. (1971). Three classes of lithification were used to describe calcareous sediments and rocks.

- Unlithified = soft sediments that have little strength and are readily deformed under the pressure of a fingernail or the broad blade of a spatula. In the classification used here, the prefix “unlithified” is used (e.g., unlithified packstone).
- Partially lithified = firm but friable sediments that can be scratched with a fingernail or the edge of a spatula blade. Here the prefix “partially lithified” is used, as in “partially lithified grainstone.”
- Lithified = hard, nonfriable, cemented rock that is difficult or impossible to scratch with a fingernail or the edge of a spatula. Here the pre-

fix “lithified” is used, as in “lithified wackestone” or “lithified coral rudstone.”

Two classes of lithification were used to describe siliclastic sediments and rocks as follows:

Soft = sediment core can be split with a wire cutter.

Hard = the core is hard (i.e., consolidated, well indurated, or cemented) if it must be cut with a hand or diamond saw. For these materials, the suffix “-stone” is added to the soft-sediment name, as in “sandstone, siltstone, and claystone.” Note that this varies from terms used to describe calcareous sediments, for which the suffix “-stone” has no firmness implications.

Core description

The visual core description (VCD) forms and barrel sheets summarize the data obtained during shipboard core description (see “[Core descriptions](#)”). Cores were described according to IODP conventions with modifications for coral-bearing sediment sequences recovered during Expedition 307. Barrel sheets represent the summarized electronic information from the VCD forms using AppleCore software.

Graphic lithology

The lithologic classification is based on a modified version of Mazzullo et al. (1988). Different sediment types are graphically represented on the barrel sheets using the symbols illustrated in [Figure F4](#).

The Graphic Lithology column can comprise a maximum of three different lithologies (for interbedded sediments) or three different components (for mixed sediments) for the same core interval. Lithology and components are quantitatively plotted in 10% intervals. Only interbedded lithologies that constitute at least 10% are displayed and represented by a vertical line dividing the lithologies. The textures of carbonates following Dunham’s 1962 classification ([Fig. F1](#)) are shown in the same column.

Bioturbation

The degrees of bioturbation are defined as “abundant,” “common,” “moderate,” “rare,” and “not evident.”

Sedimentary structures

The locations and nature of sedimentary structures are shown in the Structure column of the barrel sheets. The legend of symbols used to designate structures is shown in [Figure F4](#).

Fossils

The occurrence of macro- and microfossils is marked in a separate column. The symbol legend is shown in [Figure F4](#). For coral fragments in the cores, additional characteristics were applied. The following three stages of preservation were differentiated: good, moderate and poor. If possible, the degree of bioerosion and dissolution was estimated and noted in the VCD.

Lithologic accessories

Lithologic accessories comprise various additional sedimentary features (e.g., dropstones and cements) as listed in [Figure F4](#). Positions in the core are marked in the Accessories column by the appropriate symbol.

Core disturbance

Observations of drilling-related disturbance were recorded in the Disturbance column using the symbols shown in [Figure F4](#). The degree of drilling disturbance in soft and firm sediments is as follows:

Slightly disturbed = bedding contacts are slightly deformed.

Moderately disturbed = bedding contacts have undergone extreme bowing.

Very disturbed = bedding is completely deformed as flowing, coring/drilling slough, and other soft-sediment stretching and/or compressional shearing structures attributed to the coring/drilling.

Soupy = intervals are water-saturated and have lost all aspects of original bedding.

The degree of fracturing in indurated sediments and rocks is described using the following categories:

Slightly fractured = core pieces are in place and broken.

Moderately fractured = core pieces are in place or partly displaced, and original orientation is preserved or recognizable (drilling slurry may surround fragments [i.e., drilling/coring “biscuits” are evident]).

Highly fragmented = core pieces are probably in correct stratigraphic sequence (although they may not represent the entire sequence), but original orientation is lost.

Drilling breccia = the core is crushed and broken into many small and angular pieces with original orientation and stratigraphic position lost. Often drilling breccia is completely mixed with drilling slurry.

Smear slides and thin sections

Smear slides were analyzed for matrix compositions of the recovered sediments. The following categories were used: trace (<0.1%), rare (0.1%–1%), present (1%–5%), common (5%–20%), abundant (20%–50%), and dominant (>50%). Visual quantitative estimation of components is based on reference charts in Flügel (1982). When the sediments were too lithified for smear slide analyses, thin sections were analyzed instead. Tables containing data from smear slide and thin section analyses (see “[Core descriptions](#)”) include information about the sample location and whether the sample represents a dominant (D) or a minor (M) lithology in the core.

Samples

The positions of subsamples are indicated in the Sample column of VCD forms and barrel sheets and are abbreviated as follows: SS (smear slide), THS (thin section), PAL (micropaleontology), IW (interstitial water), XRD (X-ray diffraction), CARB (total carbon, total organic carbon), and MBIO (microbiology and geochemistry).

Color

After the core was split, color was determined visually using the Munsell Color Company (1994) color chart. In addition, color was measured with a Minolta CM-2002 spectrophotometer mounted on the AMST. These measurements were determined on the damp core surface, and clear plastic film was used to cover the core. The Minolta CM-2002 measures reflected visible light in thirty-one 10 nm wide bands ranging from 400 to 700 nm. Routine measurements were made at evenly spaced intervals within each section, taking into account section length and the position of voids within the section. Measurement spacing was 2 cm for core intervals.

Once daily, the spectrophotometer was calibrated for white color reflectance by attaching its white calibration cap. These white color calibrations were made to avoid variation in color readings due to the laboratory environment (temperature, humidity, and background light) and instrument variations. Spectrophotometer readings were recorded using Labview (version 5.0).

Digital camera imagery

A track-mounted Kodak DCS 460 digital camera was set up in the core laboratory so that complete cores or specific sections of interest could be imaged, cataloged, and stored.

Biostratigraphy

Shipboard age assignments were determined based on calcareous nannofossils and planktonic foraminifers. The microfossil assemblages were examined from core catcher samples of each core. Additionally, some critical horizons were selected to refine placement of datum levels and assemblage boundaries. Sample position, group abundance, group preservation, and species frequencies as well as age or zone of each fossil group were recorded for each sample in the Janus database.

Correlation of the nannofossil and foraminiferal zonal schemes to magnetostratigraphy are summarized in Figure F5. Datum levels are listed in Tables T2 and T3. The timescale and datum ages of planktonic foraminifers and nannofossils follow those of Berggren et al. (1995b).

Details of the shipboard methods for each microfossil group are described as follows.

Planktonic foraminifers

We applied the zonal schemes of Berggren et al. (1995a, 1995b) and Jenkins (1985, 1993). Ages of species datum levels are largely from Berggren et al. (1995a, 1995b, and references therein).

Taxonomic concepts for Neogene taxa were adopted from Kennett and Srinivasan (1983).

Sample preparation methods varied according to the degree of lithification. Unlithified sediment samples were soaked in tap water and then washed over a 63 μm sieve. Partially lithified material was soaked in a 3% H_2O_2 solution before washing. Washed samples were dried at 60°C and then sieved into the >125 μm fraction. The >125 μm fraction is used for examination of planktonic foraminifers. Planktonic foraminiferal abundances were quantitatively estimated using the following categories:

- D = dominant (>30%).
- A = abundant (10%–30%).
- F = few (5%–10%).
- R = rare (1%–5%).
- P = present (<1%).
- B = barren (no planktonic foraminifers).

Preservational characteristics were determined as follows:

- VG = very good (no evidence of breakage or dissolution).
- G = good (dissolution effects are rare; >90% of specimens unbroken).
- M = moderate (dissolution damage, such as etched and partially broken tests, occurs frequently; 30%–90% of the specimens unbroken).

P = poor (strongly recrystallized or dominated by fragments and broken or corroded specimens).

Calcareous nannofossils

The zonal scheme of Bukry (1973, 1975) with zonal code numbers added and modified by Okada and Bukry (1980), was used for Cenozoic calcareous nannofossils. The zonation scheme of Gartner (1977) was used for Pleistocene biostratigraphy, with reference to Okada and Bukry (1980), in order to obtain higher resolution for biostratigraphic correlation. This scheme is presented in Figure F6. The Cenozoic zonal schemes of Martini (1971) and Okada and Bukry (1980), together with the geomagnetic polarity timescale, are presented in Figure F5. Cenozoic biostratigraphic events, including but not limited to the zonal/subzonal indicators of Martini (1971) and their proxies, are listed in Table T2.

Standard smear slides were made of all soft lithologies. Smear slides of indurated lithologies were prepared by the traditional double-slurry smear slide method. Calcareous nannofossils were examined by means of standard microscope techniques, under cross-polarized and transmitted light at 1000 \times . We adopted a simple system to characterize preservational states:

- VG = very good (all specimens are in pristine condition and can be identified with certainty).
- G = good (little or no evidence of dissolution and/or secondary overgrowth of calcite; diagnostic characters fully preserved; all specimens can be identified).
- M = moderate (dissolution and/or secondary overgrowth; partially altered primary morphological characteristics; however, nearly all specimens can be identified at the species level).
- P = poor (severe dissolution, fragmentation, and/or secondary overgrowth with primary features largely destroyed; many specimens cannot be identified at the species level and/or generic level).

Relative abundance estimates for individual species were categorized as follows:

- D = dominant (>100 specimens of a species per field of view).
- A = abundant (10–100 specimens of a species per field of view).
- C = common (1–10 specimens per field of view).
- F = few (one specimen per 10 fields of view).
- R = rare (fewer than one specimen per 10 fields of view).
- B = barren (no calcareous nannofossils found).

Paleomagnetism

Paleomagnetic studies aboard the *JOIDES Resolution* during Expedition 307 comprised routine measurements of the natural remanent magnetization (NRM) of archive-half sections before and after alternating-field (AF) demagnetization and low-field volumetric magnetic susceptibility (k) measurements made on whole cores. The paleomagnetic measurements at Site U1317 were carried out on the whole-round sections. Tests were carried out on all sections from Hole U1316B to evaluate the feasibility of NRM measurement on whole-round sections. Freezing and splitting (see “**Introduction**”) can affect the measurements on archive-half sections, especially in carbonate-rich sediments where NRM is very weak. Moreover, by measuring on whole-round sections, the same volume is measured as for the susceptibility measurements, which is an advantage for calibration of paleointensities.

Remanence measurements and AF demagnetizations were performed using a long-core cryogenic magnetometer (2G Enterprises model 760-R). This instrument is equipped with a direct-current superconducting quantum interference device (DC-SQUID) and has an inline AF demagnetizer capable of reaching peak fields of 80 mT. The spatial resolution measured by the width at half-height of the pickup coils response is <10 cm for all three axes, although they sense a magnetization over a core length up to 30 cm. The magnetic moment noise level of the cryogenic magnetometer is $\sim 10^{-9}$ emu or 10^{-6} A/m for 10 cm³ rock volume. The practical noise level, however, is affected by the magnetization of the core liner ($\sim 8 \times 10^{-6}$ A/m) and the background magnetization of the measurement tray ($\sim 1 \times 10^{-5}$ A/m).

The NRM of archive halves or whole-round sections of all core sections was measured unless precluded or made worthless by drilling-related deformation. Measurements were made at intervals of 5 cm starting at 10 cm above and ending at 10 cm below the base. The number of demagnetization steps and the peak field used reflected the demagnetization characteristics of the sediments, the severity of the drill string magnetic overprint, the desire not to exceed peak fields of 20 mT shipboard, and the need to maintain core flow through the laboratory. One step of three-axes AF demagnetization and subsequent section measurement at 5 cm intervals takes ~ 5 min. Measurements without AF demagnetization require only 3 min. Following the NRM measurement, a two-step demagnetization was employed (~ 13 min) using peak fields of 10 and 15 mT or 15 and 20 mT. Low peak demagnetization fields ensure that the core sections remain useful for shore-based high-

resolution (U-channel) studies of magnetic remanence.

Measurements were undertaken using the standard IODP magnetic coordinate system (+x = vertical upward from the split surface of archive halves, +y = left split surface when looking upcore, and +z = downcore). Data were stored using the standard IODP file format. Void depths and otherwise disturbed intervals were manually noted on the “cryomag log sheets” and later taken into account. All sections were measured using an internal diameter setting of 6.5 cm. Background tray magnetization was measured at the beginning of each shift and subtracted from all measurements.

Full orientation was attempted using the Tensor orientation tool. The Tensor tool is rigidly mounted onto a nonmagnetic sinker bar attached to the top of the core barrel assembly. The Tensor tool consists of three mutually perpendicular magnetic field fluxgate sensors and two perpendicular gravity sensors. The information from both sets of sensors allows the azimuth and dip of the hole to be measured as well as azimuth of the APC core. The azimuthal reference line is the double orientation line on the core liner and remains on the working half after the core is split.

Where the shipboard AF demagnetization appears to have isolated the characteristic remanent magnetization, paleomagnetic inclinations and/or declinations of the highest demagnetization step (typically 15 or 20 mT) were used to make an initial designation of magnetic polarity zones. The revised timescale of Cande and Kent (1995) was used as a reference for the ages of correlative polarity chrons.

The magnetic susceptibility of whole-round sections was measured on two separate track systems. Whole-core sections were measured on the Fast Track MSCSL system to rapidly acquire magnetic susceptibility data for stratigraphic correlation. After whole cores warmed to room temperature, magnetic susceptibility measurements were made as part of MST analyses (see “[Physical properties](#)”). When time allowed, the partially demagnetized NRM intensity of selected core intervals was normalized by the MST whole-core magnetic susceptibility to assess the potential for deriving estimates of relative geomagnetic field paleointensity.

Discrete samples were collected from working halves in standard ~7 cm³ plastic cubes with orientation marks on the bottom of the sampling box pointing upcore. Intervals of coring- or drilling-related core deformation were avoided.

Geochemistry and microbiology

The objectives of shipboard geochemical and microbiological sampling during Expedition 307 were to determine the stratigraphic distribution of zones of active microbial reaction and to identify stratigraphic intervals characterized by relatively high rates of hydrocarbon fluid flow. These objectives were achieved through the development of high-resolution vertical profiles of interstitial water and headspace gas geochemistry and the acquisition of sediment samples for a wide suite of microbiological analyses. At Site U1316, depth profiles of dissolved sulfate and methane gas in Hole U1316A were used to establish a scheme for detailed microbiological and biogeochemical sampling and postcruise research in Hole U1316B. Because of drilling contingencies, detailed microbiological and biogeochemical sampling was carried out simultaneously with collection and shipboard analysis of interstitial water at Sites U1317 and U1318.

Interstitial water samples

Shipboard interstitial water samples were obtained from 5–20 cm long whole-round intervals that were cut on the catwalk, capped, and taken to the laboratory for immediate processing. In cases where the time required to obtain pore fluids exceeded the rate at which new cores arrived, interstitial water samples were stored in a refrigerator until processed. After extrusion from the core liner, the surface of each whole-round interval was carefully scraped with a spatula to remove potential contamination. Sediments were then placed in a titanium squeezer, which was modified after the standard stainless steel squeezer of Manheim and Sayles (1974). Interstitial water was passed through a prewashed Whatman number 1 filter fitted above a titanium screen, filtered through a 0.45 µm Gelman polysulfone disposable filter, and subsequently extruded into a pre-cleaned (10% HCl) 50 mL plastic syringe attached to the bottom of the squeezer assembly. After interstitial water collection, the syringe was removed to dispense aliquots for shipboard and shore-based analyses.

Interstitial water analyses

Most interstitial water samples were analyzed for routine shipboard measurements according to standard procedures (Gieskes et al., 1991). Salinity was measured as total dissolved solids using a digital refractometer. The pH was determined by ion-selective electrode. Alkalinity was determined by Gran titration with a Metrohm autotitrator. The acidified alka-

linity sample was saved for shore-based phosphate analyses.

Dissolved inorganic carbon was measured using a Coulometrics 5011 CO₂ coulometer. An aliquot of 1.0 mL of interstitial water was pipetted into the reaction tube followed by addition of 3.0 mL of 2N HCl after attaching the reaction tube to the coulometer apparatus. The liberated CO₂ was titrated, and the end point was determined by a photodetector. Measured concentrations were corrected for the value of the acid blank. Analytical uncertainty, based on repeated measurements of the International Association of the Physical Sciences of the Ocean (IAPSO) standard and reagent-grade calcium carbonate, was $\pm 1\%$.

Concentrations of chloride and sulfate were determined by manual dilution and injection into a Dionex DX-120 ion chromatograph. Chloride concentrations were also determined by titration with AgNO₃. Quantification was based on comparison with IAPSO standard seawater.

Dissolved silica and ammonium concentrations were determined by spectrophotometric methods using a Shimadzu UV Mini 1240 spectrophotometer. Concentrations of Fe, Mn, Ca, Mg, Sr, B, Li, and Ba were determined using the Jobin-Yvon Ultrace inductively coupled plasma-atomic emission spectrometer (Murray et al., 2000). Analytical standards for all elements were then prepared by analyzing mixtures of this master standard and seawater.

Gas analyses

Concentrations of methane through propane hydrocarbon gases were monitored at intervals of 1–2 samples per core. The standard gas analysis program for safety and pollution prevention purposes (Kvenvolden and McDonald, 1986) was complemented by additional headspace analyses following a slightly different approach (Iversen and Jørgensen, 1985; Hoehler et al., 2000; Shipboard Scientific Party, 2003) with the intent to better constrain the concentrations of dissolved gases. Compared to the rapid safety-oriented protocol, which measures methane dissolved in interstitial water, the latter, more time consuming alternative, measuring the additional dissolution of methane adsorbed onto sediment, provides an estimate of total methane.

For the required safety analysis, a 3 cm³ bulk sediment sample from a freshly exposed end of a core section was collected upon core removal using a brass boring tool or plastic syringe and then extruded into a 20 mL headspace vial and immediately capped with a silicone/polytetrafluoroethylene (PTFE) septum, which was sealed with an aluminum

crimp cap. The vial was then heated to 60°C for ~20 min prior to analysis.

For samples designated for refined headspace analysis, a 5 cm³ sediment sample was collected from a freshly exposed end of a core section using an open-ended plastic syringe. The sample was collected by penetrating the sediment surface while the plunger was maintained at the sediment surface to prevent contamination from atmospheric gases or trapped air bubbles. After sampling, the syringe was extruded until 3 cm³ of sample remained and the excess was shaved off with a flat spatula flush with the end of the syringe barrel to provide an accurate estimate of the sediment volume within the syringe. The remaining 3 cm³ sediment sample in the syringe was extruded into a 20 mL vial containing 5 mL of 1M NaOH. The vial was immediately capped with a silicone/PTFE septum and an aluminum crimp cap. After vigorous manual shaking for 2 min, the vials were shaken automatically for an additional hour and subsequently left to stand for at least 23 h at room temperature prior to analysis by gas chromatograph (GC).

GC analyses of headspace samples for both safety and refined protocols were performed in an identical manner. A 5 mL volume of headspace gas was extracted from the sealed sample vial using a standard gas syringe and directly injected into the GC. The headspace gas samples were analyzed using the GC3 chromatograph, a Hewlett Packard 5890 II Plus GC, equipped with an 8 ft \times 1/8 inch stainless steel column packed with HayeSep S (100–120 mesh) and a flame ionization detector (FID). Some samples were analyzed for higher molecular weight hydrocarbons by injection into the natural gas analyzer, a modified Hewlett Packard 5890 II Plus GC with an FID and a thermal conductivity detector. Concentrations of methane, ethane, ethene, propane, and propene were obtained. The carrier gas was helium, and the GC oven was programmed from 100°C (5.5 min hold) to 140°C (4 min hold) at a rate of 50°C/min. Data were processed using a Hewlett-Packard 3365 program.

The safety methane concentrations (ppm) were used to derive the concentration of dissolved methane (μM) as described by equation 1 below. Adsorbed methane ($\mu\text{mol/g}$) was calculated by subtracting the dissolved methane concentration from the total methane concentration (μM) as determined by the refined (NaOH) protocol and normalizing to mass using density and porosity relationships.

The concentration of dissolved methane, both in the safety and refined protocols, was derived from the headspace concentration by the following equation:

$$\text{CH}_4 = [(\chi_M - \chi_{\text{bkg}}) \times P_{\text{atm}} \times V_H] / (R \times T \times \phi \times V_S), \quad (1)$$

where

- V_H = volume of the sample vial headspace,
- V_S = volume of the whole sediment sample,
- χ_M = molar fraction of methane in the headspace gas (obtained from GC analysis),
- χ_{bkg} = molar fraction of methane in headspace gas because of background,
- P_{atm} = pressure in the vial headspace (assumed to be the measured atmospheric pressure when the vials were sealed),
- R = the universal gas constant,
- T = temperature of the vial headspace in degrees Kelvin, and
- ϕ = sediment porosity (determined either from moisture and density measurements on adjacent samples or from porosity estimates derived from gamma ray attenuation [GRA] data representative of the sampled interval).

Sediment analyses

Only limited analyses were carried out on sediment samples because of the short duration and emphasis on interstitial water and gas geochemistry of Expedition 307. To enable determination of carbonate mass accumulation rates, samples taken immediately adjacent to those used for determining dry bulk density were measured for inorganic carbon content using a Coulometrics 5011 CO₂ coulometer. A total of ~10–15 mg of freeze-dried, ground sediment was weighed and reacted with 2N HCl. The liberated CO₂ was titrated, and the end point was determined by a photodetector. Calcium carbonate concentration, expressed as weight percent, was calculated from the inorganic carbon content, assuming that all evolved CO₂ was derived from dissolution of CaCO₃, by the following equation:

$$\text{CaCO}_3 \text{ (wt\%)} = 8.33 \times \text{inorganic carbon (wt\%)}. \quad (2)$$

No correction was made for the presence of other carbonate minerals such as dolomite. Analytical uncertainty, based on repeated measurements of reagent-grade calcium carbonate, was ±1%.

Microbiology

Core handling and sampling

Drilling

Microbiological sampling depends on careful and appropriate sample handling techniques. Precise operational definitions for special microbiology handling terminology, such as “clean” or “sterile” are given in the “Explanatory Notes” chapter of the Leg 201 *Initial Reports* volume (Shipboard Scientific Party, 2003).

Because the samples were retrieved from stable sedimentary environments, the prokaryotes are expected to be sensitive to chemical and physical change, in particular to changes in oxygen, temperature, and pressure. Consequently, all samples for microbiology and process studies were transferred from the drilling platform to the hold refrigerator (set to <10°C) as quickly as possible and were kept as whole-core sections until processed. In order to avoid intermittent warming of retrieved cores, IODP’s usual core handling procedure was modified. Efforts were also made to obtain APC cores, even when this led to an increase in core recovery times, as APC cores are generally much less disturbed than XCB cores. RCB cores were used for deeper sections of the sites with partially-lithified to lithified sediments.

In order to ensure that we were indeed analyzing the indigenous prokaryotes and their activities, tests for contamination were conducted during the entire coring process for microbiological samples. Contamination tests were conducted in holes where microbiological sampling occurred using solutes (perfluorocarbon tracer [PFT]) or bacterial-sized particles (fluorescent microspheres) to check for potential intrusion of drill water from the periphery toward the center of the cores and thus to confirm the suitability of the core material for microbiological research. We used the chemical and particle tracer techniques described in ODP *Technical Note 28* (Smith et al., 2000a). Furthermore, the freshly collected cores were visually examined for possible cracks and other signs of disturbance by observation through the transparent core liner. Core sections observed to be disturbed before or after subsampling were not sampled further.

Sampling on the catwalk

A limited number of microbiological and related biogeochemical samples were collected on the catwalk as soon as the core was retrieved. After the core was cleaned, the core was visually inspected for signs of disturbance, such as gas voids, cracks, and drilling disturbance. One pair of sections was cut as a 2 m section and a 1 m section and the former was used for subsequent microbiological sampling. Two further sections were selected for a specific sampling request taken three times per core. The top ends of the selected sections were cut and capped (without acetone). The bottom 10–20 cm of the 2 m section was used as an interstitial water biogeochemistry sample. Samples for total prokaryotic cell counts and, where performed, PFT/fluorescent microsphere contamination checks were immediately collected using 5 cm sterile syringes from the lowermost, freshly cut end. Samples for headspace methane, $\delta^{13}\text{C}$ of methane,

and analysis of higher hydrocarbon gases were taken from the same core section or from the adjacent core top of the next section. The lowermost core end was then sealed with an end cap (without acetone). The microbiological section was quickly transported to the cold room to limit temperature increase. At Site U1318, sections destined for microbiological sampling were first run through the Fast Track MSCL. This 5 to 10 min delay allowed data for correlation purposes to be obtained before the material was sampled.

Whole-round core sampling in the cold room

A considerable proportion of the microbiological work was to be shore based because of time constraints and the necessity to use dedicated, specialized laboratory facilities. Consequently, a number of samples were taken as whole-round cores (WRCs) and stored until after the cruise. Keeping samples cool, processing times short, and minimizing contamination were key criteria for determining how the core sections were taken. To minimize changes in the microbial population, all handling took place in a cold room. The lower refrigerated core room on the hold deck of the ship served as a cold room at $<10^{\circ}\text{C}$ and was equipped with a work bench and working space for two to four persons.

Table T4 shows the cold room sample processing and cutting. For processing convenience, some of the physical property samples (e.g., oedometry and microtomography) were also sectioned in the cold room. The subsectioning equipment was the standard IODP core cutter coupled with a clean wire or blade. Samples were taken for measurement of bacterial activities (anaerobic oxidation of methane, sulfate reduction, methanogenesis, thymidine incorporation, and hydrogenase activity), capped, packed in a gas-tight aluminum bag in a nitrogen atmosphere with an oxygen scrubber sachet (Merck "Aerocult A"), and stored at 4°C . Samples for fluorescence in situ hybridization and virology were collected and stored in the same way. Samples for gas analysis were cut and sealed in a tin with Milli-Q water with the addition of 20 mL of 1% sodium azide to prevent bacterial activity. The samples for DNA, lipid biomarker, and amino acid analyses were capped, placed in polyethylene bags, and frozen in a -80°C freezer. Samples for oedometry and microtomography were capped and stored at 4°C . Standard IODP core end-cap color codes were maintained with the top of the section blue and the base of the section orange. Cut WRC samples were stored with a clear upper cap and orange lower cap indicating orientation, and the base of the residual core was capped with an orange

cap before return to the core laboratory for reintroduction into the standard core handling process.

Total cell counts

The most immediate method to visualize and quantify the deep biosphere is total prokaryotic cell counts using the nucleic acid stain acridine orange. These counts have been made on a wide range of ODP sediment cores, including cores from the Peru margin and the equatorial Pacific (Parkes et al., 1994; D'Hondt et al., 2004). In general, these counts have demonstrated an exponential decrease of prokaryotic cells with depth. The method detects sediment layers of increased cell density that often coincide with particular geochemical conditions that are conducive to prokaryote growth (Parkes et al., 2000). The AODC enumeration method was used at all sites during this leg.

Procedures and protocols

Potentially contaminated sediment was removed with a sterile scalpel. A 1 cm^3 minicore was then taken with a sterile 5 mL plastic syringe. The syringe was sealed with a sterile stopper. In a clean area of the laboratory, the 1 cm^3 plug was extruded into a sterile serum vial containing 9 mL of 2% (v/v) filter sterilized ($0.2\ \mu\text{m}$) formaldehyde in 3.5% NaCl. The vial was crimped and shaken vigorously to disperse the sediment particles.

Total prokaryotic cell numbers and numbers of dividing or divided cells were determined using acridine orange as a fluorochrome dye with epifluorescence microscopy (Fry, 1988). Fixed samples were mixed thoroughly, and a 5–20 μL subsample was added to 10 mL of 2% (v/v) formaldehyde and 2% (v/v) acetic acid filter-sterilized ($0.1\ \mu\text{m}$) in 3.5% NaCl. Acetic acid dissolves a substantial amount of carbonate, allowing larger samples to be processed, therefore increasing accuracy and giving a lower detection limit. Acridine orange (50 μL of a 1 g/L filter-sterilized [$0.1\ \mu\text{m}$] stock solution) was added, and the sample was incubated for 3 min. Stained cells and sediment were removed on a $0.2\ \mu\text{m}$ black polycarbonate membrane. Excess dye was flushed from the membrane by rinsing with a further 10 mL aliquot of 2% (v/v) filter-sterilized formaldehyde plus 2% (v/v) acetic acid in 3.5% NaCl, and the membrane was mounted for microscopic analysis in a minimum of paraffin oil under a coverslip.

Mounted membranes were viewed under incident illumination with a Zeiss Axiophot microscope fitted with a 100 W mercury vapor lamp, a wide-band interference filter set for blue excitation, a 100 \times (numerical aperture = 1.3) Plan Neofluar objective lens,

and 10× oculars. Prokaryote-shaped fluorescing objects were counted, with the numbers of cells on particles doubled in the final calculation to account for masking by sediment grains. The detection limit for prokaryotic cells was estimated at 1×10^5 cells/cm³ (Cragg, 1994).

The percentage of cells involved in division has been suggested as an indication of growth, although the assessment of dividing cells has never had a standardized approach in the literature. Dividing cells were defined operationally as those having clear invagination. A divided cell is operationally defined as a visually separated pair of cells of identical morphology. The percentage of cells involved in division is then calculated as follows:

$$\text{Percentage of cells involved in division} = \frac{[\text{number of dividing cells} + 2 (\text{number of divided cell pairs})] \times 100}{\text{total number of prokaryotic cells}}$$

Perfluorocarbon tracer contamination tests

In each hole chosen for microbiological subsampling, PFT was continuously fed into the seawater drill fluid at a tracer concentration of 1 mg/L seawater drill fluid. Concentrations of PFT were measured in all sections used for microbiological studies. A 5 cm³ subcore from the same section was routinely taken, as described by Smith et al. (2000a). Air samples were occasionally taken to monitor the ambient concentration of PFT on the catwalk. The concentrations of PFT at the outer periphery of the cores and in the drill fluid were measured to verify delivery of the PFT. During APC, the concentration of PFT was measured in a syringe sample taken adjacent to the core center. During XCB coring and RCB drilling of harder sediment, chunks of intact core adjacent to the center of the core were collected for PFT measurement, thus providing data on the minimal size and quality of intact core pieces that could be confidently sampled for microbiological investigations.

To measure PFT concentrations, we used a HP-PLOT/AL203 "S" deactivated column with film thickness = 50 μm, length = 15 m, phase ratio = 12, and column internal diameter = 0.25 mm. The inlet temperature was 180°C with 10 psi, the detector temperature was 250°C, and the column temperature was 100°C for 8 min and then ramped up 50°C/min to 200°C. The PFT peak was at a retention time of 5.7 min. We used a 1 mL injection. Larger injections resulted in loss of material.

Procedures refined during Leg 201 (Shipboard Scientific Party, 2003) were employed. The sample headspace vial was first baked at 80°C for 10 min. Clean nitrogen gas was injected onto the column to ensure that no PFT peak resulted from residual PFT in the sy-

ringe or in the GC. After a clean run was achieved, the sample was injected using a 1 mL plastic syringe. A new 1 mL syringe was used for each sample. For best results, background air samples were taken regularly from the same location used for capping headspace vials, ideally on the catwalk when no core was present.

Fluorescent microparticle tracer

The procedure for assessing particle contamination was adapted from that used during Leg 190 (Smith et al., 2000a, 2000b). A plastic bag with a suspension of micrometer-sized fluorescent spheres was positioned within the core catcher. The bead suspension was 30 mL containing 2.1×10^{11} microspheres, giving a concentration of $\sim 7 \times 10^6$ microspheres/μL. The beads were released inside the core barrel as it hit the sediment, maximizing the effectiveness of the beads as tracers of potential bacterial contamination. A 5 cm³ subcore was routinely taken from the cut core-end adjacent to the interstitial water WRC, midway between the core center and the periphery. This sample was mixed with 15 mL of saturated sodium chloride solution and shaken on a wrist-action shaker to disperse the sediment plug. The suspension was centrifuged (Marathon 10K; 5 min; 2800 × g), to separate the microspheres (density = 1) from the sediment particles. The supernatant was filtered onto black polycarbonate filters (0.2 μm pore size). Fluorescent microspheres were counted under ultraviolet light, and data are reported as number of microspheres per cubic centimeters of sediment.

Evaluating contamination tests

When comparing the results of both contamination tests (the presence of beads and PFT concentration inside 5 cm³ subcores), one should consider the following. First, in contrast to the beads, PFT can travel through very small pore spaces and is found in the laboratory air and on the hands of anyone who has handled a core liner. Therefore, although its presence at high concentrations in a sediment sample (>0.1 ng PFT/g sediment) may suggest contamination, it is not necessarily an indication that microorganisms from the drilling fluid have in fact contaminated the sample. The PFT detection limit reported for Leg 201 sites was not set as a lower limit of the ability to detect PFT by the GC, but as a lower limit of ability to confidently assess the presence of PFT in real samples given the uncertainty inherent in subtracting background levels of PFT and the reliability of the integration of small GC peaks. The absence of PFT from a sample indicates that contamination by drill water has not occurred.

Second, whereas the number of microspheres (2.1×10^{11} microspheres/30 mL bag) deployed is equivalent to the number of bacteria in ~400 L of seawater (assuming 5×10^8 bacteria/L), microsphere deployment does not produce a uniform dispersion along the core. Although PFT can usually be found in sediment samples taken from the edge of cores, the same is not true for microspheres. At this point, without knowing the factors that control the final concentration and distribution of microspheres along the core barrel, one should consider the microspheres as a qualitative rather than a quantitative measure of contamination. The presence of microspheres in sediment samples away from the edge of a core is a strong indication that contamination by prokaryote-sized particles from the drilling water has occurred, although the absence of microspheres in the contamination sample is not proof of lack of contamination in adjacent samples. However, microspheres are inert and have a historical presence, thus, any researcher receiving samples can independently check for the presence of microspheres in their specific subsamples.

Physical properties

Physical properties were measured on whole-round cores and on undisturbed portions of split cores. The MST was used on whole cores for nondestructive measurements of wet bulk density, compressional wave velocity, magnetic susceptibility, and natural gamma radiation. Magnetic susceptibility was also measured on the Fast Track MSCL before the cores were equilibrated to room temperature to allow fast stratigraphic correlation and composite depth construction (see “[Composite depths](#)”). Thermal conductivity measurements were also made on whole-round cores after the cores were thermally equilibrated. Undrained shear strength, moisture and density (MAD), and compressional wave velocity (V_p) were measured at discrete intervals on split cores, usually at a frequency of two or three per section. Figure F7 shows the sequence of physical property measurements made during Expedition 307, and Table T5 lists the average sampling intervals for each of the physical property data sets collected.

Physical property measurements gathered during Expedition 307 were used to obtain (1) high-resolution records for hole to hole correlation, construction of complete stratigraphic sequences, and downhole log calibration; (2) information related to sediment composition, diagenesis, and consolidation history to help constrain the location of unconformities; and (3) data for the calculation of synthetic seismograms (i.e., compressional wave velocity and bulk density)

and for the calculation of local heat flow (i.e., thermal conductivity).

Shipboard measurements

The Fast Track MSCL measurements were run shortly after cutting the whole-round cores on the catwalk to start the stratigraphic correlation of the different holes. To ensure thermal homogeneity for all other physical property measurements, data were collected after equilibrating the cores to ambient room temperature (17°–25°C). Detailed information on the physical principles underlying the sampling methods discussed here can be found in Blum (1997).

Fast Track MSCL

The Oregon State University Fast Track MSCL for measuring magnetic susceptibility on cores as soon as possible following recovery was first introduced during ODP Leg 202. During Expedition 307, we used the IODP Fast Track MSCL system that contains two magnetic susceptibility loops on a single track to speed up analysis time. This helped us make drilling adjustments aimed at ensuring the recovery of a complete stratigraphic section while allowing us to run the MST to optimize data quality. For a number of critical sections designated for microbiological sampling, sections were first run through the Fast Track MSCL (immediately after cutting on the catwalk) and then sent to the cool room for microbiological subsampling. This procedure ensured that at least some stratigraphic data was obtained from these cores.

Multisensor track

The MST consists of an automated track that moves whole-core sections through sensors measuring magnetic susceptibility, GRA bulk density, P -wave velocity (P -wave logger [PWL]), and natural gamma radiation (NGR). Approximately one whole-round per core section from Holes U1316B, U1316C, U1317A, U1317D, and U1318B was dedicated to microbiological analysis and was not run through the MST.

Magnetic susceptibility, GRA density, and NGR were measured on all cores regardless of collection method (i.e., APC, XCB, or RCB). P -wave velocities were measured only on the upper APC intervals because loss of coupling between the liner and core with XCB and RCB drilling resulted in inaccurate values.

P -wave velocity was measured at 5 cm intervals (5 times at 1 s period) using a 500 kHz compressional wave pulse at a repetition rate of 1 kHz. The transmitting and receiving transducers were aligned horizontally, perpendicular to the core axis. A pair of dis-

placement transducers monitored the separation between the compressional wave transducers. Sediments must completely fill the liner for the PWL to provide accurate results. PWL measurements were inaccurate at Site U1317 due to high coral content in a muddy matrix and drilling with XCB and RCB of the lower consolidated sediments, which created insufficient contact between the sediments, the core liner, and the transducers.

Magnetic susceptibility was measured using a Bartington Model MS-2 meter with an 80 mm internal diameter sensor loop (88 mm coil diameter) operating at a frequency of 565 Hz and an alternating field of 80 A/m (0.1 mT) with the sensitivity range set to 1.0 Hz. The sampling interval was 5 cm, with a period of 5 times at 1 s. The long sampling period ensured acceptable readings for the usually low magnetic susceptibility of carbonate sediments. The MS-2 meter measures relative susceptibilities, which need to be corrected for volume variations. For core (d) and coil (D) diameters of 66 and 88 mm, respectively, the corresponding correction factor for d/D is 1.48 (Blum, 1997, p. 38). During data reduction, the relative susceptibility is converted to the volume-normalized magnetic susceptibility by multiplying by $1/(1.48 \times 10^5)$, or by 0.68×10^{-5} SI units.

Natural gamma radiation is a product of the decay of radioactive isotopes, predominantly U, Th, and K. NGR was measured using four scintillation detectors arranged at 90° to each other and perpendicular to the core (as outlined by Hoppie et al., 1994). During Expedition 307, NGR was measured every 5 cm for a period of 5 times at 1 s. NGR calibration was performed at the beginning of the expedition. For the interval at the top of the hole in which pipe remained during downhole logging, the data can be used to complete and correct for the attenuation of the gamma ray wireline log collected through pipe. In open-hole logging sections, the wireline logging data could be used to calibrate the core data.

GRA was used to estimate sediment bulk density. This measurement is based on the principle that the ^{137}Cs attenuation, mainly by Compton scattering, of a collimated beam of gamma rays (produced by a ^{137}Cs source) passing through a known volume of sediment is related to material density (Boyce, 1976). During Expedition 307, the measurement interval was set at 5 cm (5 times at 1 s period). For each site, GRA and discrete sample bulk densities were compared for consistency.

Thermal conductivity

Thermal conductivity during Expedition 307 was measured using the needle probe technique with the TK04 system as described by Blum (1997). The

single-needle probe heated continuously in “full-space configuration” for soft sediments and in “half-space configuration” for hard rock. The probe was heated at 3 W/m and the temperature rise monitored. The optimal integration time for each conductivity measurement is calculated by an algorithm in the TK04 system for time units of 150 s and an evaluation time of 240 s. Thermal conductivity was reported in units of Watts per meter degrees Kelvin ($\text{W}/[\text{m}\cdot\text{K}]$), with an accuracy of 5% and a precision of 5%. Data were collected once per core (usually Section 3). For whole cores, the probe was inserted through an aperture drilled in the core liner at mid-depth in the section. Half-core rock specimens were measured for thermal conductivity using the half-space configuration. The needle probe was secured onto the flat surface of the half-core. Good coupling with the needle probes was ensured by flattening and smoothing the core surface with carbide-grit sandpaper. The samples and needles were allowed to equilibrate in a cool box. We applied this configuration for six samples from Hole U1316C (Cores 307-U1316C-5R through 9R and 11R).

Moisture and density properties

MAD measurements (water content, wet and dry bulk density, and grain density) were routinely measured using $\sim 10 \text{ cm}^3$ samples from split cores. Porosity and void ratio were calculated from phase-relation equations. Samples for MAD measurements were collected at a frequency of two per section (usually at 25 and 100 cm from the top of the section), taking care to sample undisturbed parts of the core and avoid drilling slurry and biscuits. Sampling frequency was increased as needed to characterize all significant lithologies.

Immediately after samples were collected, wet sediment mass (M_t) was measured. Samples were then placed in a convection oven for 24 h at a temperature of $105^\circ \pm 5^\circ\text{C}$. After drying, dry sediment mass (M_d) and dry sediment volume (V_d) were measured. Sample mass was determined on board to a precision of $\pm 0.01 \text{ g}$ using two Scientech 202 electronic balances to compensate for the ship’s motion. Volumes were determined using a helium five-chambered pycnometer with an approximate precision of $\pm 0.02 \text{ cm}^3$. The determination of water content followed the methods of the American Society for Testing and Materials (ASTM) designation (D) 2216 (ASTM International, 1989). The recommended equation for the water content calculation, which is the ratio of the pore fluid mass to the dry sediment mass (weight percent), is as follows:

$$W_c (\text{wt}\%) = (M_t - M_d) / (M_d - rM_d), \quad (3)$$

where

W_c = water content reported as a decimal ratio of percent dry weight, and

r = salinity.

Wet bulk density (ρ) is the density of the total sample, including pore fluid. In high-porosity sediment, bulk density was calculated using the following:

$$\rho = M_t/V_t \quad (4)$$

where V_t is the total sample volume ($\sim 10 \text{ cm}^3$).

Porosity (ϕ) was calculated using the following equation:

$$\phi = (W_c \rho)/[(1 + W_c) \rho_w], \quad (5)$$

where ρ_w is the density of the pore fluid (assuming a salinity of 35‰).

The grain density (ρ_{grain}) was calculated from dry mass and dry volume. Both values were corrected for salt using the following equation:

$$\rho_{\text{grain}} = (M_d - s)/[V_d - (s/\rho_{\text{salt}})], \quad (6)$$

where

s = salt correction and

ρ_{salt} = density of salt (2.257 g/cm^3 , assuming a salinity of 35‰).

Dry density (ρ_d) is the ratio of M_d to V_d and is used for calculations of mass accumulation. Dry density was calculated using the following equation:

$$\rho_d = (\phi/W_c) \times \rho_w. \quad (7)$$

During Expedition 307, GRA densitometer measurements on unconsolidated sediments were commonly higher than discrete density measurements. In addition, in low-porosity sediments, GRA density was usually lower, by as much as 5%, than discrete density measurements. Three explanations for these differences have been proposed (Shipboard Scientific Party, 1997):

1. The MST software does not include a correction for the attenuation effect in high-porosity sediments (Boyce, 1976; Lloyd and Moran, 1992).
2. Air trapped in the sediment-filled beakers (unconsolidated sediments) reduces the relative saturated weight and increases the relative volume measured in the pycnometer, thereby decreasing the resulting bulk density.
3. Low-porosity sediments which are semilithified to lithified have a smaller core diameter and subsequently a relatively smaller attenuating volume than the calibrated volume, which results in a lower calculated density.

To solve the first problem, GRA densities were corrected using the Boyce (1976) equation:

$$\rho = [(\rho_{bc} - \rho_{fc}) \times (\rho_g - \rho_f)]/(\rho_{gc} - \rho_{fc}) + \rho_f \quad (8)$$

where

ρ = corrected density,

ρ_{bc} = GRA density,

ρ_{fc} = fluid density calculated from gamma counts (1.128 g/cm^3),

ρ_g = true grain density of quartz (2.65 g/cm^3),

ρ_f = true fluid density (1.024 g/cm^3), and

ρ_{gc} = grain density calculated from gamma counts (2.65 g/cm^3).

It is unclear how to improve the accuracy of the MAD procedure. Therefore, it is assumed that discrete measurements are more accurate, whereas GRA density gives a reliable high-resolution relative density trend.

Sonic velocity

P-wave velocity in sediments was measured on the split core (*P*-wave sensor 3 [PWS3]; x-direction) using vertically oriented transducer pairs (500 Hz) with the upper transducer pressed against the split surface and the lower pressed against the core liner. In case of insufficient contact between the liner and the sediments, the PWS3 was applied directly on the sediment without liner. These data were recorded, digitized, and transferred to the Janus database. Core thickness was measured using a digital caliper that was directly mounted on the transducer pair. The velocity transducers were calibrated using a series of polycarbonate standards of known length. The axial pressure applied between sample and transducer was monitored by a pressure cell. To improve the coupling between transducer and sample, distilled water was applied to the transducer head. Measurements were corrected for the additional traveltime passing through the core liner. Three PWS3 measurements were usually made per section.

Undrained shear strength

The peak undrained shear strength of the unconsolidated sediment was measured at an interval of three per section using a manual Torvane shear apparatus (strength: 1 rev = 1 kg/cm²) following the procedures of Boyce (1977). In the interpretation of shear vane measurements, a cylinder of sediment is assumed to be uniformly sheared around the axis of the vane in an undrained condition with cohesion as the principal contributor to shear strength. Departures from this assumption include progressive cracking within and outside of the failing specimen, uplift of the failing core cylinder, drainage of local pore pressures, and stick-slip behavior. The shear strength measurements were taken as close as possible to the locations of the PWS3 measurements to facilitate the correlation between these parameters.

In situ temperature measurements

In situ temperature measurements were made using an APC temperature (APCT) tool. The APCT tool fits directly into the coring shoe of the APC and consists of a battery pack, data logger, and a platinum resistance-temperature device calibrated over a temperature range from 0° to 30°C. Before entering the borehole, the tool was first briefly stopped at the mudline to thermally equilibrate with bottom water. After the APC penetrated the sediment, it was held in place for 10 min as the APCT instrument recorded the temperature of the cutting shoe every 5 s. Initially, there was an instantaneous temperature rise from frictional heating caused by APC penetration. This heat, gradually dissipating into the surrounding sediments, and the equilibrium temperature of the sediments was then estimated by applying a mathematical heat-conduction model to the temperature decay record (Horai and Von Herzen, 1985). Additional information on the APCT tool can be found in previous *Initial Reports* volumes (Shipboard Scientific Party, 1992, 1994).

For shallow-water sites, a longer mudline stop was required to ensure that the temperature tools had sufficient time to equilibrate to bottom water temperatures. At deeper sites, this time was reduced as the tools are able to thermally equilibrate during descent through deeper waters with very low thermal gradients. The synthetic thermal decay curve for the APCT tool is a function of the geometry and thermal properties of the probe and the sediments (Bullard, 1954; Horai and von Herzen, 1985). However, it is never possible to obtain a perfect match between the synthetic curves and the data because (1) the probe never reaches thermal equilibrium during the penetration period; (2) contrary to theory, the frictional pulse upon insertion is never instantaneous; and (3) temperature data are sampled at discrete intervals, meaning that the exact time of penetration is always uncertain. Thus, both the effective penetration time and equilibrium temperature must be estimated by applying a fitting procedure, which involves shifting the synthetic curves in time to obtain a match with the recorded data. The data collected >20–50 s after penetration usually provide a reliable estimate of equilibrium temperature. However, where the APC has not achieved a full stroke, leakage of drilling fluid into the formation may occur and results are not considered reliable.

Composite depths

Core recovery from a single hole is generally insufficient to obtain a complete geologic section because of core-recovery gaps between successive APC, XCB, and RCB cores, despite the often apparent 100% or

more nominal recovery (Ruddiman et al., 1987; Hagelberg et al., 1995). To maximize recovery of complete geologic sections during Expedition 307, multiple holes were drilled at all sites. The degree of continuity of the recovered cores at each site was assessed by development of composite depth sections using the Splicer software, following the general methodology first used during Leg 138 (Hagelberg et al., 1992). Similar methods were used during Legs 154 (Curry, Shackleton, Richter, et al., 1995), 162 (Jansen, Raymo, Blum, et al., 1996), 167 (Lyle, Koizumi, Richter, et al., 1997), 177 (Gersonde, Hodell, Blum, et al., 1999), and Expedition 303 (Shipboard Scientific Party, 2005). This section describes the methods used to produce composite and spliced sections during Expedition 307 using Splicer software. At on-mound Site U1317, real changes in the thicknesses of stratigraphic units precluded sensible construction of a composite scale over very short distances between holes.

Composite section development

The assembly and verification of a complete composite stratigraphic section is a two-step process that requires the construction of a composite depth scale, followed by splicing.

Composite depth scale

Cores from the various holes must first be stratigraphically correlated and depth-shifted relative to each other. Such correlation enables development of a mcd scale. The mcd scale differs from the traditional (hole specific) mbsf depth scale. Mbsf is based on the length the drill string (advanced on a core-by-core basis) and is often inaccurate because of ship heave (which is not compensated in APC coring), tidal variations in sea level, and other sources of error. Depths of samples/measurements taken within the cores/sections are then constructed based on the mbsf depth of the respective core top and the cumulative length of the sections in that core. This method of depth calculation may result in apparent overlap of cores and apparent “stratigraphic reversals” because of sediment expansion in the cores (typically 5%–15%). In contrast, the mcd scale is built by assuming that the uppermost sediment (commonly referred to as the mudline) in the first core from a given hole is the sediment/water interface. This core becomes the “anchor” in the composite depth scale and is typically the only one in which depths are the same on both the mbsf and mcd scales. From this anchor, core logging data are correlated among holes downsection. For each core, a depth offset (a constant) that best aligns the observed lithologic variations to the equivalent cores in

adjacent holes is added to the mbsf depth in sequence down the holes. Depth offsets are often chosen to optimize correlation of specific features in cores from adjacent holes.

For Expedition 307, the mcd scale and the splice are based on the stratigraphic correlation of the physical properties and biostratigraphic and lithostratigraphic data as described above. Such correlation of events, involving alignment of data present in multiple holes, provides verification of the extent of recovery of the sedimentary section. The data sets were extracted from the ship's Janus database and converted into the correct format using the Splicer Integrator (version 303.0) and then imported into the Splicer software package (version 2.1). Splicer is an interactive, UNIX-based software package designed by Peter DeMenocal, Ann Esmay, and Suzanne O'Hara at Lamont-Doherty Earth Observatory (LDEO) specifically for IODP stratigraphic correlation purposes.

The data from Expedition 307 were culled to avoid the use of anomalous values resulting from voids, edge effects at section boundaries, and disturbed intervals in the cores. Magnetic susceptibility peaks provide the best lithologic parameter for correlation of Site U1316. Magnetic susceptibility (from MSC/L or MST), natural gamma ray emission, and GRA density are useful parameters for correlation.

Splicer software allows for direct graphical and statistical comparison of data from each hole. Tie lines are drawn between correlative features present in the data (data excursions, peaks, troughs, and plateaus). The software calculates the statistical correlation over an adjustable depth range (typically ± 2 m), to aid the visual correlation process. No depth adjustments (stretching or squeezing) are made. Because depth intervals within cores are not squeezed or stretched by Splicer, not all correlative features can be aligned exactly. Stretching or squeezing between cores from different holes may reflect small-scale differences in sedimentation and/or distortion caused by the coring and archiving processes. The tops of APC cores are generally stretched and the bottoms compressed, although this is dependent on lithology. In addition, sediment (especially unconsolidated mud, sand, gravel, and coral pieces at Site U1317) occasionally falls from higher levels in the borehole onto the tops of cores as they are recovered, and, as a result, the uppermost 20–40 cm of many cores is not reliable. Where possible, tie points were chosen in the middle to lower portion of cores, where the record is likely to have been least disturbed by expansion or other erroneous effects. Utilization of at least two different physical properties allows hole to hole correlations to be made with

greater confidence than would be possible with only a single parameter. Core photographs and VCDs were also a useful reference source for identifying potentially correlative lithologic features within cores. Where overlapping data from other holes were unavailable, causing data gaps in the total section, the depth adjustment applied was the cumulative offset from the overlying aligned cores. The resulting adjusted depth scale is called the mcd, and the section produced by the aligned cores is termed a composite depth section.

All adjustments to the data were written to a data output file. The offset column allows conversion of sample depths from mbsf to mcd, effectively creating a sampling strategy guide. The mcd for any point within a core equals the mbsf depth plus the offset. A table is presented in each site chapter summarizing core offsets for conversion from mbsf to mcd scales.

Splicing

Splicer software allows the user to merge, or splice, the best data from the composite section to produce a single spliced record representing the complete geologic section at each site. The spliced record is constructed by patching the intervals missing in a single hole with data from adjacent holes. This process provides a single representative record of the physical properties parameters (e.g., magnetic susceptibility, spectral reflectance, or GRA bulk density) for the entire section, which is ideally suited to guide core sampling for high-resolution paleoenvironmental studies.

Splice tie points were made between adjacent holes where visually obvious features are strongly correlated. The choice of tie points (and hence of a splice) is a somewhat subjective exercise. Our method in the construction of a splice followed these three rules:

1. Where possible, avoid using the uppermost and lowermost 1 m of cores, where disturbance resulting from drilling artifacts (even if not apparent in core logging data) is most likely.
2. Attempt to incorporate those portions of the recovered core that are most representative of the overall stratigraphic section of the site.
3. Minimize tie points to simplify sampling.

The splice operation is depth-constrained so that no further core offset is possible. Because of core expansion and/or compression, the total length of the spliced record depends on which intervals of core are selected to construct it. Each splice is constructed by beginning at the mudline at the top of the composite section and working downward. As in the composite section construction, no compression or expansion of the data are possible. Adjustments to the

composite or spliced sections, such as a linear compression of the mcd scale within individual core intervals, are required to align all features exactly (e.g., Hagelberg et al., 1995).

Depths in splice tables versus Janus depths

The depth of a core interval recorded for a tie point in a splice table is not always the same as the depth for the same core interval returned by most database queries. This is because the tie point depth is based on the liner length, which is measured when the cores are cut into sections on the catwalk. The cores are analyzed on the MST almost immediately after this liner-length measurement. At some later time, typically 10–36 h after being analyzed by the MST, core sections are split and analyzed further (see “[Core handling and analysis](#)”). At this time, the section lengths are measured again and are archived as “curated lengths.” General database queries return depths based on the curated liner lengths. Because the sections are usually expanding during the period between the two measurements, the curated length is almost always longer than the initial liner length. Thus, the depths associated with the MST data used to construct the splice table are not identical to the final depths the database assigns to a given interval. This leads to small differences (usually between 0 and 5 cm) between the mbsf and mcd recorded in a splice table and the depths reported in other places for the same core interval. We have chosen not to change these depths to be compatible with Janus because this would not improve their accuracy. For consistency, we recommend that all postcruise depth models use or build on mcd values provided in the Janus database.

Downhole measurements

Downhole logging tools are used to determine physical, chemical, and structural properties of the formation penetrated by drilling. Data are rapidly collected, continuous with depth, and, most importantly, are measured in situ. Logs may be interpreted in terms of the stratigraphy, lithology, mineralogy, and geochemical composition of the penetrated formation. Where core recovery is good, logging and core data are complementary and should be integrated and interpreted jointly, with logging data providing in situ ground truth for core data. Where core recovery is incomplete or disturbed, logging data may provide the only means to characterize the borehole section.

Downhole logs record formation properties on a scale that is intermediate between those obtained from laboratory measurements on core samples and

geophysical surveys. They are critical for calibrating geophysical survey data (e.g., through synthetic seismograms), providing the necessary link for the integration of core depth domain to seismic time domain data. Through logs, data collected at the borehole scale can be extended to a regional scale using geophysical surveys, a crucial point for paleoenvironmental (climatic and oceanographic) reconstructions.

Wireline logging was conducted at all three sites cored during Expedition 307. To accommodate for the length of the tool string, logged holes were deepened by ~30–50 m with respect to targeted depth. Downhole logging operations began after the hole had been cored and flushed with a viscous drilling mud. The drilling assembly was then pulled up to ~90–60 mbsf, and the logging tools were passed through the drill pipe into the open hole. The logging tools are joined together into tool strings so that compatible tools are run together. Each tool string was lowered separately to the base of the hole and then measurement took place as the tool string was raised at a near-constant cable speed between 275 and 500 m/h (see the “Downhole measurements” sections in the individual site chapters). A wireline heave compensator (WHC) was used to minimize the effect of the ship’s heave on the tool position in the borehole (Goldberg, 1990). Further information on the procedures and wireline tools used during Expedition 307 can be found at iodp.ldeo.columbia.edu/TOOLS_LABS/index.html.

Wireline logging tool strings

Data were obtained by a variety of Schlumberger and LDEO logging tools, which were combined into the following tool strings (Fig. F8; Table T6):

1. The triple combination (triple combo) tool string consists of the Hostile Environment Gamma Ray Sonde (HNGS), Accelerator Porosity Sonde (APS), Hostile Environment Litho-Density Sonde (HLDS), Dual Induction Tool (DIT), Environmental Measurements Sonde (EMS), and the LDEO Temperature/Acceleration/Pressure (TAP) tool.
2. The Formation MicroScanner (FMS)-sonic tool string consists of the Scintillation Gamma Ray Tool (SGT), Dipole Sonic Imager (DSI), General Purpose Inclinator Tool (GPIT), and the micro-resistivity FMS.
3. The Well Seismic Tool (WST) consists of one geophone pressed against the borehole wall that is used to record the acoustic waves generated by an air gun located near the sea surface, offset by ~10 m from the ship. No marine mammals were ob-

served during or immediately prior to use of the air gun. The WST was only run in Hole U1317D.

Principles and uses of the logging tools

The properties measured by each tool, sampling intervals, and vertical resolutions are described and summarized in Table T6. Explanations of tool name acronyms and their measurement units are summarized in Table T7. More detailed descriptions of individual logging tools and their geological applications can be found in Ellis (1987), Goldberg (1997), Rider (1996), Schlumberger (1989, 1994), Serra (1984, 1986, 1989), and the LDEO-Borehole Research Group (BRG) Wireline Logging Services Guide (1994).

Data acquisition

Each tool string contains a telemetry cartridge facilitating communication between the tools and the Schlumberger Minimum Configuration Multitasking (MCM) acquisition and imaging system unit located on the ship along the wireline (seven-conductor cable). Ship heave motion is a further complication in the acquisition of quality wireline logging data. To overcome this, the wireline is fed over the WHC. As the ship heaves in the swell, an accelerometer located near the ship's center of gravity measures the movement and feeds the data, in real time, to the WHC. The WHC responds to the ship's heave by adding or removing cable slack to decouple the movement of the ship from the tool string (Goldberg, 1990). During each logging run, incoming data are recorded and monitored in real time on the MCM logging computer.

Natural radioactivity

Two wireline spectral gamma ray tools, the HNGS and the SGT, were used during Expedition 307 to measure and classify natural radioactivity in the formation and to provide a common reference for correlation and depth shifting between multiple logging runs. The HNGS uses two bismuth germanate scintillation detectors for high tool precision. It measures the natural gamma radiation from K, Th, and U isotopes and uses a 256-window spectroscopic analysis to determine concentrations of radioactive ^{40}K (in weight percent), ^{232}Th (in parts per million), and ^{238}U (in parts per million).

The SGT uses a sodium iodide scintillation detector to measure the total natural gamma ray emissions from ^{40}K , ^{238}U , and ^{232}Th in the formation. The SGT is not a spectral tool but provides high-resolution total gamma ray data for depth correlation between logging runs. It is included in the FMS-sonic tool string

to provide a reference log to correlate depth between different logging runs.

In a general manner, the radius of investigation depends on several factors: hole size, mud density, formation bulk density (denser formations display a slightly lower radioactivity), and the energy of the gamma rays (a higher-energy gamma ray can reach the detector from deeper in the formation). The HNGS data are corrected for hole size during logging.

Density

Formation density was determined with the HLDS. The tool contains a radioactive ^{137}Cs gamma ray source (662 keV) and far and near gamma ray detectors mounted on a shielded skid that is pressed against the borehole wall. Gamma rays emitted by the source experience both Compton scattering and photoelectric absorption. Compton scattering involves the ricochet of gamma rays off electrons in the formation via elastic collision, transferring energy to the electron in the process. The number of scattered gamma rays that reach the detectors is directly related to the number of electrons in the formation, which, in turn, is related to bulk density. Porosity may also be derived from this bulk density if the matrix (grain) density is known. As mentioned earlier, the HLDS also measures photoelectric absorption of the gamma rays which occurs when they reach <150 keV after being repeatedly scattered by electrons in the formation. Photoelectric absorption varies according to the chemical composition of the formation (Gardner and Dumanoir, 1980). For example, the photoelectric effect factor of calcite = 5.08 b/e-, illite = 3.03 b/e-, quartz = 1.81 b/e-, and kaolinite = 1.49 b/e-. Good contact between the tool and borehole wall is essential for acquisition of quality HLDS logs. Poor contact results in an underestimation of density values. Both density correction and caliper measurement of the hole are used to check the contact quality.

Porosity

Formation porosity was measured with the APS. The sonde incorporates a minitron neutron generator that produces fast neutrons (14.4 MeV) and five neutron detectors (four epithermal and one thermal) positioned at differing distances from the minitron. The measurement principle involves counting neutrons that arrive at the detectors after being slowed by neutron absorbers surrounding the tool. The highest energy loss occurs when neutrons collide with hydrogen nuclei that have practically the same mass as the neutron (the neutrons simply bounce off heavier elements without losing much energy). If the hydrogen (i.e., water) concentration is small, as in

low-porosity formations, neutrons can travel farther before being captured and the count rates increase at the detector. The opposite effect occurs when the water content is high. Because hydrogen bound in minerals such as clays or hydrocarbons also contributes to the measurement, the raw porosity value is often overestimated. Upon reaching thermal energies (0.025 eV), the neutrons are captured by the nuclei of Cl, Si, B, and other elements, resulting in a gamma ray emission. This neutron capture cross section (Σ_t) is also measured by the tool.

Electrical resistivity

The DIT was used to provide three measures of electrical resistivity, each with a different depth of investigation into the formation. The two induction devices (deep and medium depths of penetration) transmit high-frequency alternating currents through transmitter coils, creating magnetic fields that induce secondary currents in the formation. These currents produce a new inductive signal, which is measured by the receiving coil and is proportional to the conductivity of the formation. The measured conductivities are then converted to resistivity (measured in ohm-meters). For the shallow-penetration resistivity, the current necessary to maintain a constant voltage drop across a fixed interval is measured. This is a direct measurement of resistivity. Sand grains and hydrocarbons are electrical insulators, whereas ionic solutions (i.e., pore waters) and clays are conductors. Electrical resistivity can therefore be used to evaluate porosity (by Archie's law) and fluid salinity.

Temperature, acceleration, and pressure

Downhole temperature, acceleration, and pressure were measured with the TAP tool. It was attached to the bottom of the triple combo tool string and run in memory mode with the data stored in built-in memory. After the logging run was complete, the TAP tool was removed from the tool string and returned to the downhole measurements laboratory where the data were downloaded.

The TAP tool has a dual-temperature measurement system for identification of both rapid temperature fluctuations and temperature gradients. A thin fast-response thermistor detects small, abrupt changes in temperature, and the thicker slow-response thermistor more accurately estimates temperature gradients and thermal regimes. A pressure transducer is used to activate the tool at a specified depth, typically 200 m above seafloor. A one-axis accelerometer measures tool movement downhole, which provides data for analyzing the effects of heave on the deployed tool string. The acceleration log can, in prin-

ciple, be used to correct the logging depths for the effects of heave. The temperature record must be interpreted with caution because the elapsed time between the end of drilling and the logging operation is generally not sufficient to allow the borehole to reach thermal equilibrium following circulation of the drilling fluid. The fluid temperature recorded under such circumstances may differ significantly from the temperature of the formation. Nevertheless, it is possible to identify abrupt temperature changes that may represent localized fluid flow into the borehole indicative of fluid pathways and fracturing and/or breaks in the temperature gradient that may correspond to contrasts in permeability at lithologic boundaries. For comparison and calibration of the TAP tool, drilling mud temperature was also measured with the Schlumberger EMS.

Acoustic velocity

The DSI measures transit times between sonic transmitters and an array of eight receivers. It averages replicate measurements, thus providing a direct measurement of sound velocity through sediments that is relatively free from the effects of formation damage and borehole enlargement (Schlumberger, 1989). The tool contains the monopole transmitters found on most sonic tools, but also has two crossed-dipole transmitters, providing shear wave velocity measurement in addition to the compressional wave velocity, even in slow formations (~1600 m/s).

Formation MicroScanner

The FMS provides high-resolution electrical resistivity images of the borehole wall (~30% of a 25 cm diameter borehole can be imaged on each pass). The development of the FMS tool has added a new dimension to wireline logging (Luthi, 1990; Lovell et al., 1998). The vertical resolution of FMS images is ~5 mm, allowing features such as clasts, thin beds, bioturbation, and corals to be imaged. The tool has four orthogonal arms with pads, each containing 16 button electrodes that are pressed against the borehole wall during the recording (Fig. F8). The electrodes are arranged in two diagonally offset rows of eight electrodes. A focused current is emitted from the button electrodes into the formation with a return electrode located near the top of the tool. The intensity of current passing through the button electrodes is measured. The maximum extension of the caliper arms is 15 inches, so in holes or parts of holes with a larger diameter, the pad contact will be inconsistent and the FMS images may appear out of focus and too conductive. Irregular borehole walls will also adversely affect the image quality if they lead to poor pad/wall contact. Processing transforms these mea-

surements, which reflect the microresistivity variations of the formation, into continuous, spatially oriented, high-resolution images that map the geologic structures of the borehole wall. Features such as bedding, fracturing, slump folding, and bioturbation can be resolved, and spatially oriented images allow fabric analysis and bed orientations to be measured. Local contrasts in FMS images were improved by applying a dynamic normalization to the FMS data. In such a normalization procedure, a linear gain is applied that keeps a constant mean and standard deviation within a sliding window of 2 m.

Accelerometry and magnetic field measurements

Three-component acceleration and magnetic field measurements were made with the GPIT. The primary purpose of this tool is to determine the acceleration and orientation of the FMS-sonic tool string during logging. This provides a means of correcting the FMS images for rotation and irregular vertical tool motion, allowing the true dip and direction (azimuth) of structures to be determined.

Check shot survey

A check shot survey (or zero-offset vertical seismic profile) is a type of borehole seismic survey designed to measure the seismic traveltime from the surface to a known depth. *P*-wave velocity of the formations encountered in a wellbore can be measured directly by lowering a geophone to each formation of interest, sending out a source of energy from the ship using an air gun, and recording the resultant signal. The data can then be used to convert depth to traveltime and improve the absolute values of the sonic log. It differs from a vertical seismic profile in the number and density of receiver depths recorded; geophone positions may be widely and irregularly located in the wellbore, whereas a vertical seismic profile usually has numerous geophones positioned at closely and regularly spaced intervals in the wellbore.

Wireline logging and data quality

Logging data quality may be seriously degraded by changes in the hole diameter and in sections where the borehole diameter greatly decreases or is washed out. Deep-investigation measurements such as resistivity and sonic velocity are least sensitive to borehole conditions. Nuclear measurements (density and neutron porosity) are more sensitive because of their shallower depth of investigation and the effect of drilling fluid volume on neutron and gamma ray attenuation. Corrections can be applied to the original data to reduce these effects. Natural gamma radia-

tion data provide a depth correlation between logging runs. Logs from different tool strings may, however, still have residual depth mismatches caused by ship heave during recording.

Logging depth scale

The depth of the wireline-logged measurement is determined from the length of the logging cable extended from the winch on the ship. When possible, the seafloor is identified on the natural gamma ray log by the abrupt reduction in gamma ray count at the water/sediment boundary (mudline). The coring depth (drillers depth) is determined from the known length of the bottom-hole assembly and pipe stands, and the mudline, which is usually recovered in the first core from the hole.

Discrepancies between the drillers depth of recovered core and the wireline log depth occur because of core expansion, incomplete core recovery, incomplete heave compensation, drill pipe stretch in the case of drill pipe depth, cable stretch (~1 m/km), and cable slip in the case of logging depth. Tidal changes in sea level will also have an effect. To minimize the wireline tool motion caused by ship heave, the WHC adjusts for rig motion during wireline logging operations. The small but significant differences between drill pipe depth and logging depth should be taken into account when using the logs for correlation between core and logging data. The depths of core data sets, such as density and natural gamma radiation, can be correlated with the equivalent downhole logs using programs such as Sagan, which allows mapping of the core depths onto the logging depth scale. Precise core-log depth matching may be difficult in zones where core recovery is low because of the inherent ambiguity of placing the recovered section within the cored interval. Where complete core recovery (by a composite depth splice) (Hagelberg et al., 1992) is achieved, core depths can be corrected by correlation with the logging data.

Logs from different wireline tool strings will also have slight depth mismatches. Distinctive features recorded by the natural gamma tools (HNGS or SGT), run on every tool string (except the WST), provide relative depth offsets and a means of depth shifting for correlation between logging runs.

Logging data flow and processing

Data for each logging run were recorded, stored digitally, and monitored in real time using the MCM software. On completion of logging in each hole, data acquisition preprocessing by the Schlumberger engineer is carried out; data are subsequently transferred to the downhole measurements laboratory

and transmitted via satellite to LDEO-BRG for on-shore processing. Data processing at LDEO-BRG consists of:

1. Depth matching the logs to a common reference, usually the pass covering the greatest interval;
2. Depth-shifting all logs relative to a common datum (i.e., seafloor);
3. Making corrections specific to individual tools; and
4. Quality control.

Once processed at LDEO-BRG, logging data were transmitted back to the ship, providing data processing in a matter of days. Processed data were then replotted on board (see the “Downhole measurements” sections in each site chapter). Further postcruise processing of the FMS data is performed at LDEO-BRG. Postcruise-processed acoustic, caliper, density, gamma ray, magnetic, neutron porosity, resistivity, and temperature data are available in ASCII, with FMS images as GIF files directly from the IODP U.S. Implementing Organization, Science Services-LDEO Internet World Wide Web site at iodp.ldeo.columbia.edu/DATA/IODP/index.html. Schlumberger GeoQuest’s GeoFrame software package is used for most of the processing. A summary of “logging highlights” is posted on the LDEO-BRG Web site at the end of each expedition.

Core-log-seismic integration

The aim of creating a synthetic seismogram is to provide a means of matching the reflections expected from the formation (measured physical properties from logging and core sources) with those in the seismic data (Mayer et al., 1985). This allows the seismic data to be interpreted in terms of the measured formation properties. For example, lithologic or chronologic boundaries can be picked out as specific reflectors. If a synthetic seismogram can be done for the three sites, they provide the basis for fine tuning the regional seismic stratigraphy.

A synthetic seismic log is a presentation of the data contained in a sonic log in the form of a seismic trace. The high-frequency data of the sonic log are replayed at the low frequency of the seismic data. A seismic section is the result of acoustic reflections from subsurface strata. The reflections depend on the contrasts of the acoustic impedances (i.e., velocity \times density) of the adjacent layers, that is, the reflection coefficient (R). When both a sonic and a density log are run in a well, the acoustic impedances of the layers logged can be calculated.

Velocity and density data are required to produce the synthetic seismograms and are only produced in

downhole logging once the tool string has exited the drill pipe, typically at ~60–80 mbsf. Because of this, the core data, corrected for rebound (increased length with reduced density [e.g., Hamilton, 1976]) and temperature increase, has to be spliced onto the top of the logging data in order to provide full-depth velocity and density data sets. These full-depth data sets can then be imported into the IESX module of the Schlumberger GeoQuest program GeoFrame to calculate the synthetic seismograms.

References

- ASTM International, 1989. Standard test method for laboratory miniature vane shear test for saturated fine-grained clayey soil (Standard D4648–87). In *Annual Book of ASTM Standards for Soil and Rock* (Vol. 04.08): Philadelphia (Am. Soc. Testing and Mater.), 868–873.
- Backman, J., 1986. Late Paleocene to middle Eocene calcareous nannofossil biochronology from the Shatsky Rise, Walvis Ridge and Italy. *Palaeoogeogr., Palaeoclimatol., Palaeoecol.*, 57:43–59. doi:10.1016/0031-0182(86)90005-2
- Backman, J., 1987. Quantitative calcareous nannofossil biochronology of middle Eocene through early Oligocene sediment from DSDP Sites 522 and 523. *Abh. Geol. Bundesanst. (Austria)*, 39:21–31.
- Berggren, W.A., Hilgen, F.J., Langereis, C.G., Kent, D.V., Obradovich, J.D., Raffi, I., Raymo, M.E., and Shackleton, N.J., 1995a. Late Neogene chronology: new perspectives in high-resolution stratigraphy. *Geol. Soc. Am. Bull.*, 107:1272–1287. doi:10.1130/0016-7606(1995)107<1272:LNCNPI>2.3.CO;2
- Berggren, W.A., Kent, D.V., and Flynn, J.J., 1985. Jurassic to Paleogene, Part 2. Paleogene geochronology and chronostratigraphy. In Snelling, N.J. (Ed.), *The Chronology of the Geological Record*. Geol. Soc. London Mem., 10:141–195.
- Berggren, W.A., Kent, D.V., Flynn, J.J., and van Couvering, J.A., 1985. Cenozoic geochronology. *Geol. Soc. Am. Bull.*, 96:1407–1418. doi:10.1130/0016-7606(1985)96<1407:CG>2.0.CO;2
- Berggren, W.A., Kent, D.V., Swisher, C.C., III, and Aubry, M.-P., 1995b. A revised Cenozoic geochronology and chronostratigraphy. In Berggren, W.A., Kent, D.V., Aubry, M.-P., and Hardenbol, J. (Eds.), *Geochronology, Time Scales and Global Stratigraphic Correlation*. Spec. Publ.—SEPM (Soc. Sediment. Geol.), 54:129–212.
- Berggren, W.A., Kent, D.V., and Van Couvering, J.A., 1985. The Neogene, Part 2. Neogene geochronology and chronostratigraphy. In Snelling, N.J. (Ed.), *The Chronology of the Geological Record*. Geol. Soc. London Mem., 10:211–260.
- Blow, W.H., 1969. Late middle Eocene to Recent planktonic foraminiferal biostratigraphy. In Brönnimann, P., and Renz, H.H. (Eds.), *Proc. First Int. Conf. Planktonic Microfossils, Geneva, 1967*: Leiden (E.J. Brill), 1:199–422.
- Blum, P., 1997. Physical properties handbook: a guide to the shipboard measurement of physical properties of deep-sea cores. *ODP Tech. Note*, 26 [Online]. Available

- from World Wide Web: <http://www-odp.tamu.edu/publications/tnotes/tn26/INDEX.HTM>.
- Boyce, R.E., 1976. Definitions and laboratory techniques of compressional sound velocity parameters and wet-water content, wet-bulk density, and porosity parameters by gravimetric and gamma-ray attenuation techniques. *In* Schlanger, S.O., Jackson, E.D., et al., *Init. Repts. DSDP*, 33: Washington (U.S. Govt. Printing Office), 931–958.
- Boyce, R.E., 1977. Deep Sea Drilling Project procedures for shear strength measurement of clayey sediment using modified Wykeham Farrance laboratory vane apparatus. *In* Barker, P.F., Dalziel, I.W.D., et al., *Init. Repts. DSDP*, 36: Washington (U.S. Govt. Printing Office), 1059–1068.
- Bukry, D., 1973. Low-latitude coccolith biostratigraphic zonation. *In* Edgar, N.T., Saunders, J.B., et al., *Init. Repts. DSDP*, 15: Washington (U.S. Govt. Printing Office), 685–703.
- Bukry, D., 1975. New Miocene to Holocene stages in the ocean basins based on calcareous nannoplankton zones. *In* Kulm, L.D., von Huene, R., et al. (Eds.), *Late Neogene Epoch Boundaries*: New York (Am. Mus. Nat. Hist., Micropaleontology Press), 162–166.
- Bullard, E.C., 1954. The flow of heat through the floor of the Atlantic Ocean. *Proc. R. Soc. London A*, 222:408–429.
- Cande, S.C., and Kent, D.V., 1995. Revised calibration of the geomagnetic polarity timescale for the Late Cretaceous and Cenozoic. *J. Geophys. Res.*, 100:6093–6095. [doi:10.1029/94JB03098](https://doi.org/10.1029/94JB03098)
- Cragg, B.A., 1994. Bacterial profiles in deep sediment layers from the Lau Basin (Site 834). *In* Hawkins, J., Parson, L., Allan, J., et al., *Proc. ODP, Sci. Results*, 135: College Station, TX (Ocean Drilling Program), 147–150.
- Curry, W.B., Shackleton, N.J., Richter, C., et al., 1995. *Proc. ODP, Init. Repts.*, 154: College Station, TX (Ocean Drilling Program).
- D'Hondt, S.D., Jørgensen, B.B., Miller, D.J., Batzke, A., Blake, R., Cragg, B.A., Cypionka, H., Dickens, G.R., Fardelman, T., Hinrichs, K.-H., Holm, N.G., Mitterer, R., Spivack, A., Wang, G., Bekins, B., Engelen, B., Ford, K., Gettemy, G., Rutherford, S.D., Sass, H., Skilbeck, C.G., Aiello, I.W., Guerin, G., House, C., Inagak, F., Meister, P., Naehr, T., Niitsuma, S., Parkes, R.J., Schippers, A., Smith, D.C., Teske, A., Wiegel, J., Naranjo Padillo, C., and Solis Acosta, J.L., 2004. Distributions of microbial activities in deep seafloor sediments. *Science*, 306:2216–2221. [doi:10.1126/science.1101155](https://doi.org/10.1126/science.1101155)
- Dunham, R.J., 1962. Classification of carbonate rocks according to depositional texture. *In* Ham, W.E. (Ed.), *Classification of Carbonate Rocks*. AAPG Mem., 108–121.
- Ellis, D.V., 1987. *Well Logging for Earth Scientists*: New York (Elsevier).
- Embry, A.F., and Klovan, J.E., 1971. A late Devonian reef tract on northeastern Banks Island, Northwest Territories. *Bull. Can. Pet. Geol.*, 19:730–781.
- Erba, E., Premoli Silva, I., and Watkins, D.K., 1995. Cretaceous calcareous plankton biostratigraphy of Sites 872 through 879. *In* Haggerty, J.A., Premoli Silva, I., Rack, F., and McNutt, M.K. (Eds.), *Proc. ODP, Sci. Results*, 144: College Station, TX (Ocean Drilling Program), 157–169.
- Flügel, E., 1982. *Microfacies Analysis of Limestones*: Berlin (Springer-Verlag).
- Fry, J.C., 1988. Determination of biomass. *In* Austin, B. (Ed.), *Methods in Aquatic Bacteriology*: Chichester (Wiley), 27–72.
- Gardener, J.S., and Dumanoir, J.L., 1980. Litho-density log interpretation. *Trans. SPWLA Annu. Logging Symp.*, 21:1–23.
- Gartner, S., 1977. Calcareous nannofossil biostratigraphy and revised zonation of the Pleistocene. *Mar. Micropaleontol.*, 2:1–25. [doi:10.1016/0377-8398\(77\)90002-0](https://doi.org/10.1016/0377-8398(77)90002-0)
- Gealy, E.L., Winterer, E.L., and Moberly, R., Jr., 1971. Methods, conventions, and general observations. *In* Winterer, E.L., Riedel, W.R., et al., *Init. Repts. DSDP*, 7 (Pt. 1): Washington (U.S. Govt. Printing Office), 9–26.
- Gersonde, R., Hodell, D.A., Blum, P., et al., 1999. *Proc. ODP, Init. Repts.*, 177 [CD-ROM]. Available from: Ocean Drilling Program, Texas A&M University, College Station, TX 77845-9547, U.S.A. [HTML]
- Gieskes, J.M., Gamo, T., and Brumsack, H., 1991. Chemical methods for interstitial water analysis aboard JOIDES Resolution. *ODP Tech. Note*, 15 [Online]. Available from World Wide Web: http://www-odp.tamu.edu/publications/tnotes/tn15/f_chem1.htm.
- Goldberg, D., 1990. Test performance of the Ocean Drilling Program wireline heave motion compensator. *Sci. Drill.*, 1:206–209.
- Goldberg, D., 1997. The role of downhole measurements in marine geology and geophysics. *Rev. Geophys.*, 35:315–342. [doi:10.1029/97RG00221](https://doi.org/10.1029/97RG00221)
- Hagelberg, T., Shackleton, N., Pisias, N., and Shipboard Scientific Party, 1992. Development of composite depth sections for Sites 844 through 854. *In* Mayer, L., Pisias, N., Janecek, T., et al., *Proc. ODP, Init. Repts.*, 138 (Pt. 1): College Station, TX (Ocean Drilling Program), 79–85.
- Hagelberg, T.K., Pisias, N.G., Shackleton, N.J., Mix, A.C., and Harris, S., 1995. Refinement of a high-resolution, continuous sedimentary section for studying equatorial Pacific Ocean paleoceanography, Leg 138. *In* Pisias, N.G., Mayer, L.A., Janecek, T.R., Palmer-Julson, A., and van Andel, T.H. (Eds.), *Proc. ODP, Sci Results*, 138: College Station, TX (Ocean Drilling Program), 31–46.
- Hamilton, E.L., 1976. Variations of density and porosity with depth in deep sea sediments. *J. Sediment. Petrol.*, 46:280–300.
- Hoehler, T.M., Borowski, W.S., Alperin, M.J., Rodriguez, N.M., and Paull, C.K., 2000. Model, stable isotope, and radiotracer characterization of anaerobic methane oxidation in gas hydrate-bearing sediments of the Blake Ridge. *In* Paull, C.K., Matsumoto, R., Wallace, P.J., and Dillon, W.P. (Eds.), *Proc. ODP, Sci. Results*, 164: College Station, TX (Ocean Drilling Program), 79–85. [HTML]
- Hoppie, B.W., Blum, P., and the Shipboard Scientific Party, 1994. Natural gamma-ray measurements on ODP cores: introduction to procedures with examples from Leg 150. *In* Mountain, G.S., Miller, K.G., Blum, P., et al., *Proc. ODP, Init. Repts.*, 150: College Station, TX (Ocean Drilling Program), 51–59.
- Horai, K., and Von Herzen, R.P., 1985. Measurement of heat flow on Leg 86 of the Deep Sea Drilling Project. *In*

- Heath, G.R., Burckle, L.H., et al., *Init. Repts. DSDP*, 86: Washington (U.S. Govt. Printing Office), 759–777.
- Iversen, N., and Jørgensen, B.B., 1985. Anaerobic methane oxidation rates at the sulfate–methane transition in marine sediments from Kattegat and Skagerrak (Denmark). *Limnol. Oceanogr.*, 30:944–955.
- Jansen, E., Raymo, M.E., Blum, P., et al., 1996. *Proc. ODP, Init. Repts.*, 162: College Station, TX (Ocean Drilling Program).
- Jenkins, D.G., 1985. Southern mid-latitude Paleocene to Holocene planktic foraminifera. In Bolli, H.M., Saunders, J.B., and Perch-Nielsen, K. (Eds.), *Plankton Stratigraphy*: Cambridge (Cambridge Univ. Press), 263–282.
- Jenkins, D.G., 1993. Cenozoic southern mid- and high-latitude biostratigraphy and chronostratigraphy based on planktonic foraminifera. In Kennett, J.P., and Warnke, D.A. (Eds.), *The Antarctic Paleoenvironment: A Perspective on Global Change*. Antarct. Res. Ser., 60:125–144.
- Kennett, J.P., and Srinivasan, M.S., 1983. *Neogene Planktonic Foraminifera: A Phylogenetic Atlas*: Stroudsburg, PA (Hutchinson Ross).
- Kvenvolden, K.A., and McDonald, T.J., 1986. Organic geochemistry on the JOIDES Resolution—an assay. *ODP Tech. Note*, 6.
- Lamont-Doherty Earth Observatory-Borehole Research Group, 1994. *Wireline Logging Services Guide*: Lamont-Doherty Earth Observatory-Borehole Research Group.
- Lloyd, J., and Moran, K., 1992. ODP GRAPE evaluation: a report to the JOIDES Shipboard Measurements Panel. *Internal Rep., Ocean Drilling Program*.
- Lovell, M.A., Harvey, P.K., Brewer, T.S., Williams, C., Jackson, P.D., and Williamson, G., 1998. Application of FMS images in the Ocean Drilling Program: an overview. In Cramp, A., MacLeod, C.J., Lee, S.V., and Jones, E.J.W. (Eds.), *Geological Evolution of Ocean Basins: Results from the Ocean Drilling Program*. Geol. Soc. Spec. Publ., 131:287–303.
- Luthi, S.M., 1990. Sedimentary structures of clastic rocks identified from electrical borehole images. In Hurst, A., Lovell, M.A., and Morton, A.C. (Eds.), *Geological Applications of Wireline Logs*. Spec. Publ.—Geol. Soc. London, 48:3–10.
- Lyle, M., Koizumi, I., Richter, C., et al., 1997. *Proc. ODP, Init. Repts.*, 167 [Online]. Available from World Wide Web: http://www-odp.tamu.edu/publications/167_IR/167TOC.HTM.
- Manheim, F.T., and Sayles, F.L., 1974. Composition and origin of interstitial waters of marine sediments, based on deep sea drill cores. In Goldberg, E.D. (Ed.), *The Sea* (Vol. 5): *Marine Chemistry: The Sedimentary Cycle*: New York (Wiley), 527–568.
- Martini, E., 1971. Standard Tertiary and Quaternary calcareous nannoplankton zonation. In Farinacci, A. (Ed.), *Proc. 2nd Int. Conf. Planktonic Microfossils Roma*: Rome (Ed. Tecnosci.), 2:739–785.
- Mayer, L.A., Shipley, T.H., Theyer, F., Wilkens, R.H., and Winterer, E.L., 1985. Seismic modeling and paleoceanography at Deep Sea Drilling Project Site 574. In Mayer, L., Theyer, F., Thomas, E., et al., *Init. Repts. DSDP*, 85: Washington (U.S. Govt. Printing Office), 947–970.
- Mazzullo, J.M., Meyer, A., and Kidd, R.B., 1988. New sediment classification scheme for the Ocean Drilling Program. In Mazzullo, J.M., and Graham, A.G. (Eds.), *Handbook for shipboard sedimentologists. ODP Tech. Note*, 8:45–67.
- Munsell Color Company, Inc., 1994. *Munsell Soil Color Chart* (Revised ed.): Newburgh, MD (Munsell Color).
- Murray, R.W., Miller, D.J., and Kryc, K.A., 2000. Analysis of major and trace elements in rocks, sediments, and interstitial waters by inductively coupled plasma–atomic emission spectrometry (ICP–AES). *ODP Tech. Note*, 29 [Online]. Available from World Wide Web: <http://www-odp.tamu.edu/publications/tnotes/tn29/INDEX.HTM>.
- Okada, H., and Bukry, D., 1980. Supplementary modification and introduction of code numbers to the low-latitude coccolith biostratigraphic zonation (Bukry, 1973; 1975). *Mar. Micropaleontol.*, 5:321–325. doi:10.1016/0377-8398(80)90016-X
- Parkes, R.J., Cragg, B.A., Bale, S.J., Getliff, J.M., Goodman, K., Rochelle, P.A., Fry, J.C., Weightman, A.J., and Harvey, S.M., 1994. Deep bacterial biosphere in Pacific Ocean sediments. *Nature (London, U. K.)*, 371:410–413. doi:10.1038/371410a0
- Parkes, R.J., Cragg, B.A., and Wellsbury, P., 2000. Recent studies on bacterial populations and processes in marine sediments: a review. *Hydrogeol. Rev.*, 8:11–28.
- Rider, M.H., 1996. *The Geological Interpretation of Well Logs* (2nd ed.): Caithness (Whittles Publishing).
- Ruddiman, W.F., Cameron, D., and Clement, B.M., 1987. Sediment disturbance and correlation of offset holes drilled with the hydraulic piston corer: Leg 94. In Ruddiman, W.F., Kidd, R.B., Thomas, E., et al., *Init. Repts. DSDP*, 94 (Pt. 2): Washington (U.S. Govt. Printing Office), 615–634.
- Schlumberger, 1989. *Log Interpretation Principles/Applications*: Houston (Schlumberger Educ. Services), SMP–7017.
- Schlumberger, 1994. *IPL Integrated Porosity Lithology*: Houston (Schlumberger Wireline and Testing), SMP-9270.
- Serra, O., 1984. *Fundamentals of Well-Log Interpretation* (Vol. 1): *The Acquisition of Logging Data*: Dev. Pet. Sci., 15A: Amsterdam (Elsevier).
- Serra, O., 1986. *Fundamentals of Well-Log Interpretation* (Vol. 2): *The Interpretation of Logging Data*. Dev. Pet. Sci., 15B: Amsterdam (Elsevier).
- Serra, O., 1989. *Formation MicroScanner Image Interpretation*: Houston (Schlumberger Educ. Services), SMP-7028.
- Shepard, F.P., 1954. Nomenclature based on sand-silt-clay ratios. *J. Sediment. Petrol.*, 24:151–158.
- Shipboard Scientific Party, 1992. Explanatory notes. In Davis, E.E., Mottl, M.J., Fisher, A.T., et al., *Proc. ODP, Init. Repts.*, 139: College Station, TX (Ocean Drilling Program), 55–97.
- Shipboard Scientific Party, 1994. Explanatory notes. In Mountain, G.S., Miller, K.G., Blum, P., et al., *Proc. ODP, Init. Repts.*, 150: College Station, TX (Ocean Drilling Program), 21–42.

- Shipboard Scientific Party, 1997. Explanatory notes. In Eberli, G.P., Swart, P.K., Malone, M.J., et al., *Proc. ODP, Init. Repts.*, 166: College Station, TX (Ocean Drilling Program), 43–65. [PDF]
- Shipboard Scientific Party, 2003. Explanatory Notes, In D'Hondt, S.L., Jørgensen, B.B., Miller, D.J., et al., *Proc. ODP, Init. Repts.*, 201, 1–103 [CD-ROM]. Available from: Ocean Drilling Program, Texas A&M University, College Station, TX 77845-9547, USA. [HTML]
- Shipboard Scientific Party, 2005. North Atlantic climate: ice sheet–ocean atmosphere interactions on millennial timescales during the late Neogene–Quaternary using a paleointensity-assisted chronology for the North Atlantic. *IODP Prel. Rept.*, 303. doi:10.2204/iodp.pr.303.2005
- Smith, D.C., Spivack, A.J., Fisk, M.R., Haveman, S.A., Staudigel, H., and ODP Leg 185 Shipboard Scientific Party, 2000a. Methods for quantifying potential microbial contamination during deep ocean coring. *ODP Tech. Note*, 28 [Online]. Available from World Wide Web: <http://www-odp.tamu.edu/publications/tnotes/tn28/INDEX.HTM>.
- Smith, D.C., Spivack, A.J., Fisk, M.R., Haveman, S.A., Staudigel, H., and ODP Leg 185 Shipboard Scientific Party, 2000b. Tracer-based estimates of drilling-induced microbial contamination of deep sea crust. *Geomicrobiol. J.*, 17:207–219.
- Wentworth, C.K., 1922. A scale of grade and class terms of clastic sediments. *J. Geol.*, 30:377–392.

Publication: 14 October 2006

MS 307-102



Figure F1. The Dunham (1962) classification of limestones according to depositional texture, as modified by Embry and Klovan (1971) and adapted to the carbonate sediments drilled during Expedition 307. Rudstone and floatstone can be autochthonous or allochthonous.

Allochthonous carbonates original components not organically bound during deposition				Allochthonous or Autochthonous		Autochthonous limestones, original components organically bound during deposition		
Less than 10% >2 mm components				Greater than 10% >2 mm components		Boundstone		
Contains lime mud (<0.02 mm)			No lime mud	Matrix supported	>2 mm component supported	By organisms that act as bafflers	By organisms that encrust and bind	By organisms that build a rigid framework
Mud supported		Grain supported						
Less than 10% grains (>0.02 mm to <2 mm)	Greater than 10% grains							
Mudstone	Wackestone	Packstone	Grainstone	Floatstone	Rudstone	Bafflestone	Bindstone	Framestone

Figure F2. Udden-Wentworth grain-size classification of terrigenous sediments (from Wentworth, 1922).

Millimeters (mm)	Micrometers (μm)	Phi (ϕ)	Wentworth size class
4096		-12.0	Boulder
256		-8.0	Cobble
64		-6.0	Pebble
4		-2.0	Granule
2.00		-1.0	Very coarse sand
1.00		0.0	Coarse sand
1/2	500	1.0	Medium sand
1/4	250	2.0	Fine sand
1/8	125	3.0	Very fine sand
1/16	63	4.0	Coarse silt
1/32	31	5.0	Medium silt
1/64	15.6	6.0	Fine silt
1/128	7.8	7.0	Very fine silt
1/256	3.9	8.0	Clay
0.00006	0.06	14.0	

Figure F3. Diagram showing classification scheme used for siliciclastic sediments and rocks during Expedition 307 (after Shepard, 1954).

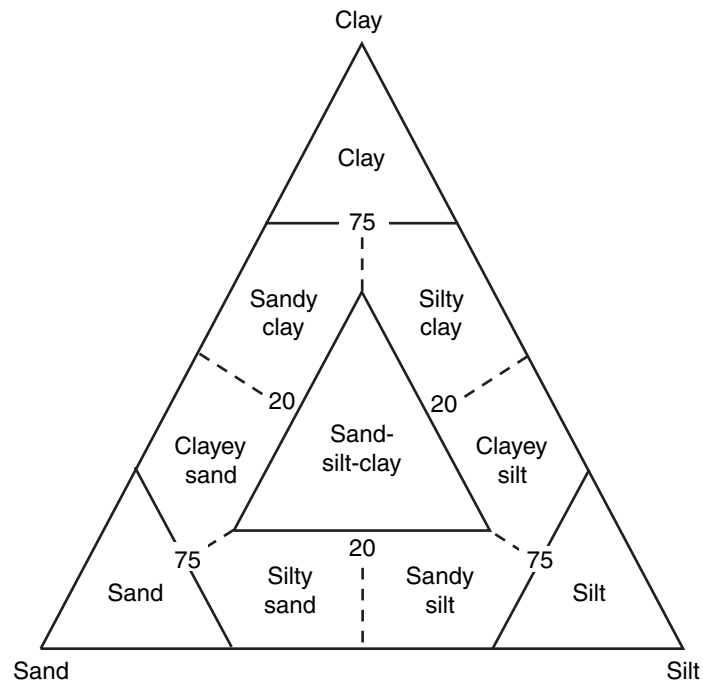


Figure F4. Key to symbols used in core description forms. (Continued on next two pages.)

Lithology

Calcareous sediment

 Mudstone	 Grainstone	 Boundstone	 Bafflestone
 Wackestone	 Floatstone	 Framestone	 Lost core
 Packstone	 Rudstone	 Bindstone	

Siliciclastic sediment

 Sand or sandstone	 Silt or siltstone	 Shale (fissile)	 Breccia
 Silty sand	 Sandy silt	 Silty clay	 Gravel
 Clayey sand	 Clayey silt	 Sandy clay	 Conglomerate
 Sand-silt-clay	 Siliceous clay/Claystone	 Clay or claystone	 Coal and peat

Contacts

 Sharp	 Scoured	 Bioturbated	 Stylolite
 Undulating	 Faulted	 Inclined	 Uncertain
 Firmground	 Hardground		

Sedimentary Structures

 Climbing ripple	 High-angle tabular bedding	 Fining upward
 Cross lamination	 Hummocky cross-strat.	 Coarsening upward
 Current ripple	 Imbrication	 Planar lamination
 Flaser bedding	 Low-angle tabular bedding	 Planar tabular bedding
 Herringbone cross-strat.	 Oscillatory ripple	 Reactivation surface
 Chaotic bedding	 Graded bedding	 Trough cross-strat.
 Convolute bedding	 Reverse-graded bedding	 Wavy parallel bedding
 Mud cracks	 Lenticular bedding	 Slump
 Birdseye structure, keystone vug		 Cone in cone structure
		 Double mud drapes

Figure F4 (continued).

Core disturbance

- Slightly disturbed
- Moderately disturbed
- Very disturbed
- Soupy

- Biscuit
- Gas expansion

- Slightly fractured
- Moderately fractured
- Highly fragmented
- Breccia

Bioturbation

- Abundant
- Common
- Moderate
- Rare
- Barren

Lithification

- Extreme (lithified)
- Moderate (partially lithified)
- Unconsolidated (unlithified)

Fossils

- Algae (undifferentiated)
- Algal stromatolite
- Asteroid
- Bivalve
- Brachiopod
- Bryozoa (delicate branching)
- Bryozoa (encrusting)
- Bryozoa (fenestrate)
- Bryozoa (tubelike)
- Calcisphere
- Cephalopod
- Coral (colonial)
- Coral (solitary)

- Crinoid
- Diatoms
- Echinoderm
- Fish remains
- Fish scale
- Fossil ghost
- Fossil fragment
- Foraminifer (large benthic)
- Foraminifer (planktonic)
- Foraminifer (small benthic)
- Foraminifer (undifferentiated)
- Gastropod
- Mollusk (undifferentiated)

- Ostracode
- Plant remains
- Pteropod
- Scolecodont
- Serpulid
- Shell fragment
- Spicule
- Spine
- Sponge
- Spore, pollen
- Radiolarian
- Rhodolith
- Vertebrate

Ichnofossils

- Bored hardground
- Chondrites
- Escape trace
- Undefined burrow

- Ophiomorpha*
- Palaeophycus*
- Planolites*
- Rhizocorallium*

- Taenidium*
- Teichichnus*
- Thalassinoides*
- Zoophycos*

Figure F4 (continued).

Lithologic accessories

	Ash layer		Dolomitic		Shale lamina
	Breccia horizon		Organic shale lamina		Silt lamina
	Calcareous		Pebbles/Granules		Sand lamina
	Charcoal fragments		Rip-up clasts		Pebbles/Granules/Sand
	Calcite concretion		Ferruginous concretion		Nodule/Concretion
	Chalcedony/Chert concretion		Hematite concretion		Pyrite concretion
	Dolomite concretion		Ikaite		Siderite concretion
	Cherty	Lth	Lithic	Sid	Siderite
Ch	Chlorite	Mc	Micaceous	Sm	Smectite
Fl	Feldspathic	Py	Pyrite	S	Sulfur
Fe	Ferruginous	Q	Quartz crystals	wf	Wood fragments
Gl	Glauconitic				
	Coated grains		Peloids		Pisolites
	Fecal pellets				
	Calcite cement		Dropstone		Mottled
	Cement, general		Gas hydrate		Mud clasts
	Clast imbrication		Lithoclast		Stromatactis
	Black spots				

Figure F5. Quaternary through Paleocene chronostratigraphic units correlated with planktonic foraminifer and calcareous nannofossil zonations and the geomagnetic polarity timescale. Timescales are from Berggren et al. (1995a) for the Cenozoic. Biozones are those of (1) Berggren et al. (1995a), (2) Blow (1969), (3) Jenkins (1985, 1993), (4) Martini (1971), and (5) Okada and Bukry (1980). Black bars = normal polarity, white bars = reversed polarity.

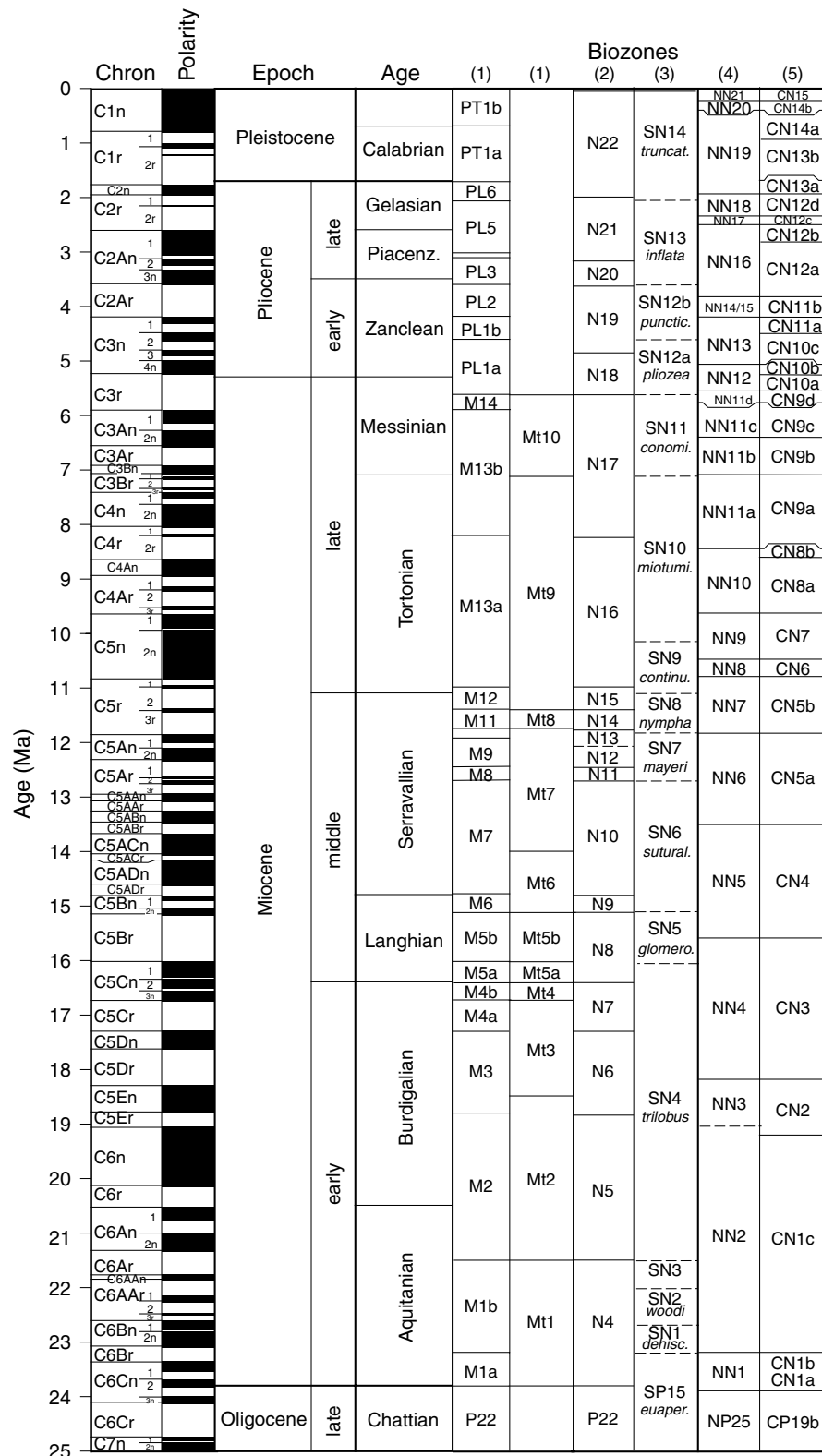


Figure F6. Quaternary calcareous nannofossil zonal scheme (after Gartner [1977]). FO = first occurrence, LO = last occurrence.

<i>Emiliana huxleyi</i> acme Zone	<i>E. huxleyi</i> acme
<i>Emiliana huxleyi</i> Zone	FO <i>E. huxleyi</i> (*0.26 m.y., +CN15)
<i>Gephyrocapsa oceanica</i> Zone	LO <i>P. lacunosa</i> (*0.46 m.y., +CN14b)
<i>Pseudoemiliana lacunosa</i> Zone	LO small <i>Gephyrocapsa</i> (*0.96 m.y.)
small <i>Gephyrocapsa</i> Zone	
<i>Helicosphaera sellii</i> Zone	LO <i>H. sellii</i> (*1.22 m.y.)
<i>Calcidiscus macintyreii</i> Zone	LO <i>C. macintyreii</i> (*1.59 m.y.)
<i>Discoaster brouwerii</i> Zone	LO <i>D. brouwerii</i> (*1.95 m.y., +CN13a)

* ages derived from Berggren (1995a)

+ equivalent zones from Okada and Bukry (1980)

Figure F7. Core-flow of physical properties. GRA = gamma ray attenuation, PWS = *P*-wave sensor.

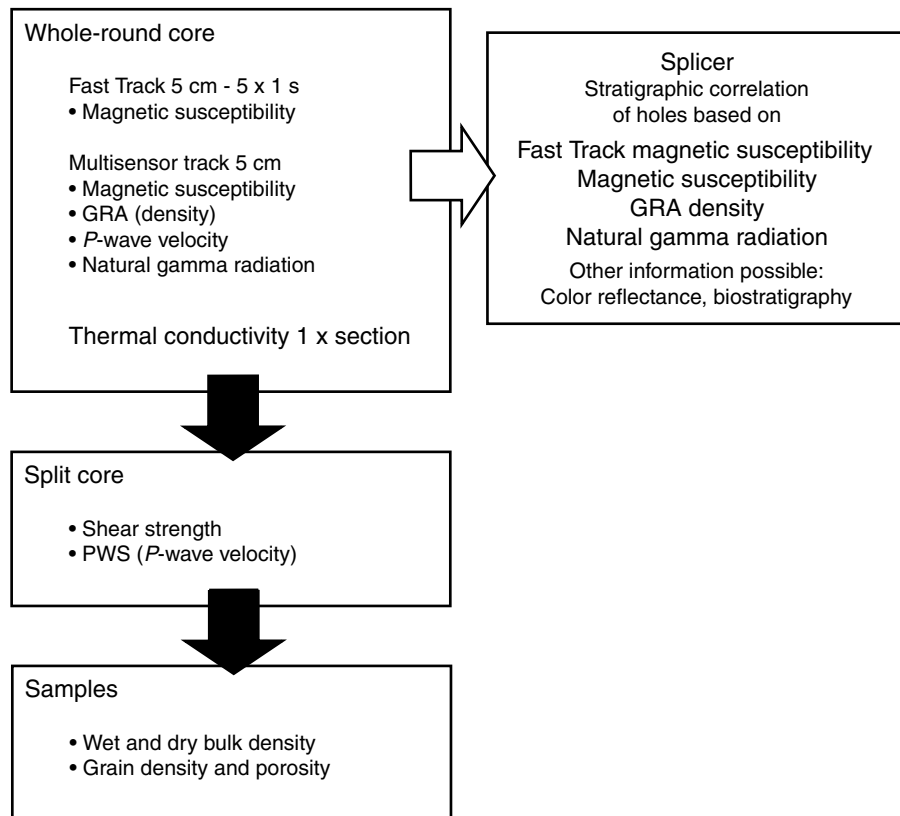


Figure F8. Schematic illustration of the configurations of tool strings used during Expedition 307. HNGS = Hostile Environment Gamma Ray Sonde, BGO = Bismuth Germanate, APS = Accelerator Porosity Sonde, HLDS = Hostile Environment Litho-Density Sonde, EMS = Environment Measurement Sonde, DIT-E = Dual Induction Tool model E, TAP = Temperature/Acceleration/Pressure, FMS = Formation MicroScanner, SGT = Scintillation Gamma Ray Tool, DSI = Dipole Sonic Imager, GPIT = General Purpose Inclinator Tool, WST = Well Seismic Tool.

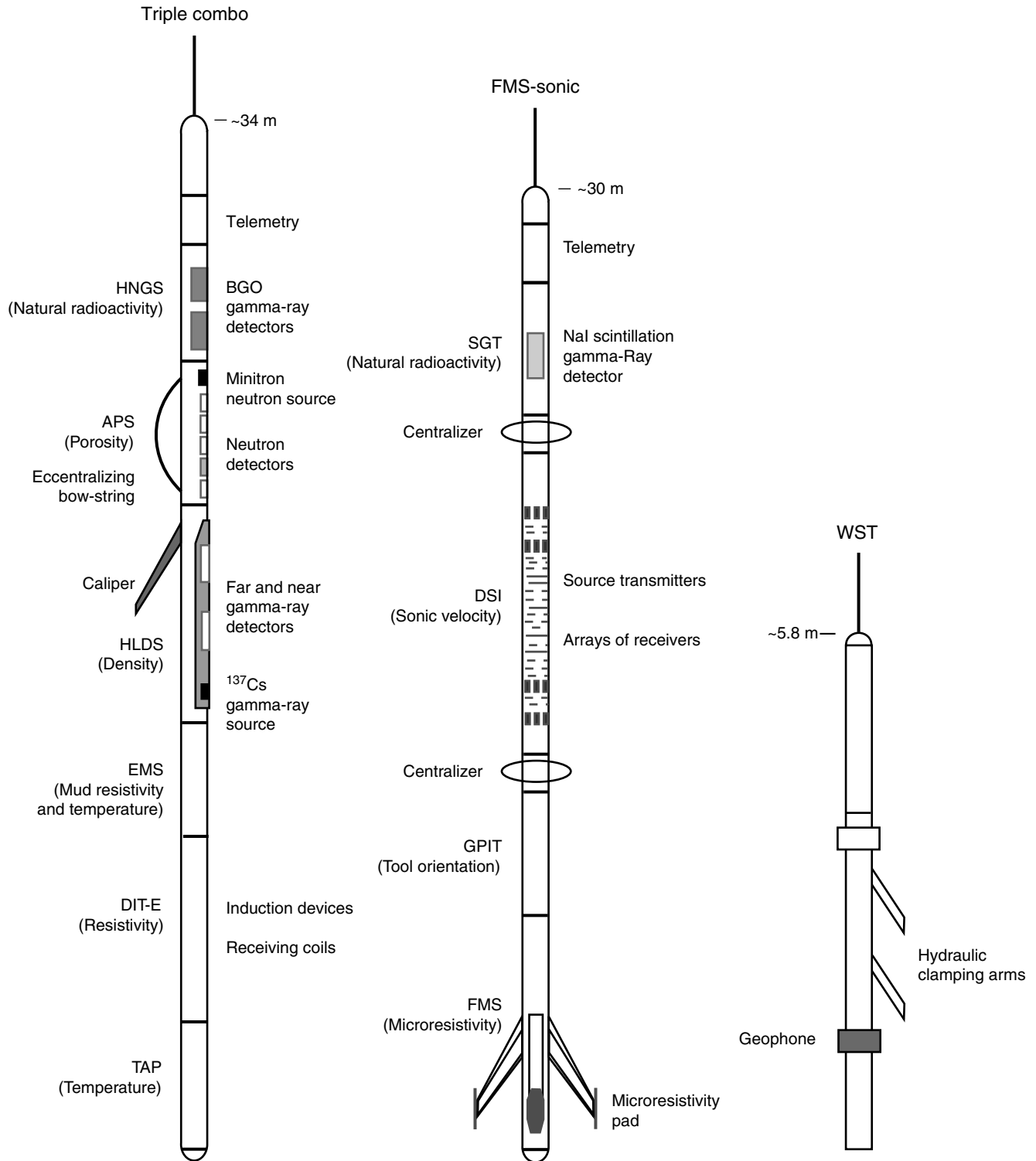


Table T1. Lithologic description of granular sediments.

Sediment class	Major modifiers	Principal names	Minor modifiers
Carbonate	<ol style="list-style-type: none"> 1. Composition of skeletal and neritic grains present in major amounts 2. Texture of clastic grains present in major amounts 	<ol style="list-style-type: none"> 1. Mudstone 2. Wackestone 3. Packstone 4. Grainstone 5. Floatstone 6. Rudstone 7. Boundstone 	<ol style="list-style-type: none"> 1. Composition of skeletal grains present in minor amounts 2. Texture of clastic grains present in minor amounts
Siliciclastic	<ol style="list-style-type: none"> 1. Composition of all grains present in major amounts 2. Grain fabric (gravels only) 3. Grain shape (optional) 4. Sediment color (optional) 	<ol style="list-style-type: none"> 1. Gravel 2. Sand 3. Silt 4. Clay, etc. 	<ol style="list-style-type: none"> 1. Composition of all grains present in minor amounts 2. Texture and composition of siliciclastic grains present as matrix (for coarse-grained clastic sediments)

Table T2. Ages of planktonic foraminifer datum levels. (See table notes. Continued on next two pages.)

Event	Zone (base)	Age (Ma)	Reference
T <i>Globorotalia flexuosa</i>		0.07	Joyce et al., 1990
B <i>Bolliella calida</i>		0.22	Chaproniere et al., 1994
T <i>Globoquadrina pseudofoliata</i>		0.22	Chaproniere et al., 1994
B <i>Globorotalia flexuosa</i>		0.4	Joyce et al., 1990
B <i>Globorotalia hirsuta</i>		0.45	Pujol and Duprat, 1983
T <i>Globorotalia tosaensis</i>	Pt1b	0.65	Srinivasan and Sinha, 1992
B <i>Globorotalia crassaformis hessi</i>		0.75	Chaproniere et al., 1994
T <i>Pulleniatina finalis</i>		1.4	Chaproniere et al., 1994
T <i>Globigerinoides fistulosus</i>	Pt1a	1.77	Berggren et al., 1995b
T <i>Globigerinoides extremus</i>		1.77	Berggren et al., 1985
Pliocene/Pleistocene boundary			
		1.77	
B <i>Globorotalia truncatulinoides</i>		2	Zijderveld et al., 1991
B <i>Globorotalia truncatulinoides</i>	(SN14)		Jenkins, 1993
T <i>Globorotalia exilis</i> (Atlantic)		2.15	Berggren et al., 1985
T <i>Globorotalia miocenica</i>	PI6	2.3	Berggren et al., 1995b
T <i>Neogloboquadrina atlantica</i>		2.41	Weaver and Clement, 1987
T <i>Globorotalia puncticulata</i> (Atlantic)		2.41	Zijderveld et al., 1991
T <i>Globorotalia pertenuis</i>		2.6	Berggren et al., 1985
T <i>Dentoglobigerina altispira</i>	PI5	3.09	Berggren et al., 1995b
T <i>Globorotalia multicamerata</i>		3.09	Berggren et al., 1985
T <i>Sphaeroidinellopsis seminulina</i>	PI4	3.12	Berggren et al., 1995b
B <i>Sphaeroidinella dehiscens</i> s.s.		3.12	Weaver and Clement, 1987
B <i>Globorotalia inflata</i>	(SN13)	3.2*	Jenkins, 1993; Chaproniere et al., 1995
T <i>Globorotalia</i> sp. cf. <i>G. crassula</i> (North Atlantic)		3.25	Berggren et al., 1985
B <i>Globorotalia pertenuis</i>		3.33	Berggren et al., 1985
B <i>Globorotalia miocenica</i> (Atlantic)		3.45	Berggren et al., 1985
T <i>Globorotalia margaritae</i>	PI3	3.58	Berggren et al., 1995b
T <i>Pulleniatina primalis</i>		3.58	Srinivasan and Sinha, 1992
<i>Pulleniatina</i> transition s/d		3.65	Berggren et al., 1985
T <i>Pulleniatina spectabilis</i>		3.95	Berggren et al., 1985
T <i>Globoturborotalita nepenthes</i>	PI2	4.18	Berggren et al., 1995a
B <i>Globorotalia puncticulata</i>		4.2	Berggren et al., 1985
B <i>Globorotalia crassaformis</i>		4.5	Weaver and Clement, 1987
T <i>Globigerinoides seiglei</i>		4.5	Chaproniere et al., 1994
T <i>Globorotalia cibaensis</i>	PI1b	4.6	Berggren et al., 1995b
B <i>Sphaeroidinella dehiscens</i> s.l.		4.7	Berggren et al., 1985
B <i>Globorotalia margaritae</i>		5.2	Srinivasan and Sinha, 1992
Miocene/Pliocene boundary			
		5.25	
T <i>Globorotalia tumida</i>		5.32	Srinivasan and Sinha, 1992
B <i>Globorotalia tumida</i>	PI1a	5.6	Chaproniere et al., 1994
B <i>Globorotalia sphericomiozea</i>		5.6	Srinivasan and Sinha, 1992
B <i>Globorotalia pliozea</i>		5.6	Srinivasan and Sinha, 1992
B <i>Globorotalia pliozea</i>		5.6	Berggren et al., 1985
B <i>Globorotalia puncticulata</i>	(SN12)	5.3*	Jenkins, 1993; Chaproniere et al., 1995
B <i>Globorotalia tumida</i>		5.6	Berggren et al., 1985
T <i>Globoquadrina dehiscens</i>		5.6	Chaproniere et al., 1994
T <i>Globoquadrina dehiscens</i>		5.8	Berggren et al., 1985
T <i>Globorotalia languaensis</i>	M14	6	Chaproniere et al., 1994
B <i>Globorotalia margaritae</i>		6	Chaproniere et al., 1994
B <i>Neogloboquadrina acostaensis</i> transition s/d		6	Chaproniere et al., 1994
B <i>Globorotalia margaritae</i>		6.2	Srinivasan and Sinha, 1992
B <i>Pulleniatina primalis</i>		6.4	Chaproniere et al., 1994
B <i>Globorotalia menardii</i> form 5		6.4	Chaisson and Leckie, 1993
B <i>Neogloboquadrina acostaensis</i> transition d/s		6.4	Srinivasan and Sinha, 1992
B <i>Neogloboquadrina atlantica</i> transition d/s		6.6	Srinivasan and Sinha, 1992
B <i>Globorotalia conomiozea</i>		6.8	Spiegler and Jansen, 1989
B <i>Globorotalia conomiozea</i>	(SN11)	7.12*	Jenkins, 1993; Chaproniere et al., 1995
B <i>Globorotalia menardii</i> form 5		7.12	Krijgsman et al., 1994
T <i>Globorotalia menardii</i> form 4		7.2	Krijgsman et al., 1994
B <i>Globorotalia suterae</i>		7.4	Krijgsman et al., 1994
B <i>Globorotalia cibaensis</i>		7.8	Glacon et al., 1990
B <i>Globorotalia juanai</i>		7.8	Chaisson and Leckie, 1993
B <i>Candeina nitida</i>		8.1	Chaisson and Leckie, 1993
B <i>Globigerinoides extremus</i> / <i>Globorotalia plesiotumida</i>	M13b	8.3	Berggren et al., 1995b
T <i>Neogloboquadrina continuosa</i>	(SN10)		Jenkins, 1993
B <i>Neogloboquadrina humerosa</i>		8.5	Berggren et al., 1985
B <i>Neogloboquadrina pachyderma</i>		9.2	Berggren, 1992

Table T2 (continued).

Event	Zone (base)	Age (Ma)	Reference
T <i>Neogloboquadrina nympha</i>		10.1	Berggren, 1992
T <i>Neogloboquadrina nympha</i>	(SN9)		Jenkins, 1993
B <i>Neogloboquadrina acostaensis</i>	M13	10.9	Berggren et al., 1995b
B <i>Neogloboquadrina acostaensis</i>		10.9	Miller et al., 1991
T <i>Neogloboquadrina mayeri</i>	M12	11.4	Miller et al., 1994
T <i>Neogloboquadrina mayeri</i>	(SN8)		Jenkins, 1993
B <i>Globoturborotalita nepenthes</i>	M11	11.8	Blow, 1979
B <i>Globoturborotalita nepenthes</i>		11.8	Miller et al., 1994
T <i>Globorotalia panda</i>		11.8	Berggren, 1993
T <i>Globorotalia fohsi robusta</i>	M10	11.9	Berggren et al., 1985
T <i>Globorotalia praescitula</i>		11.9	Berggren, 1992
T <i>Globorotalia fohsi lobata</i>		12.1	Wright and Miller, 1992
B <i>Neogloboquadrina mayeri</i>	(SN7)	12.1*	Jenkins, 1993; Chaproniere et al., 1995
B <i>Globorotalia fohsi robusta</i>	M9b	12.3	Berggren, 1992
T <i>Tenuitella clemenciae</i>		12.3	Li et al., 1992
T <i>Tenuitella minutissima</i>		12.3	Li et al., 1992
T <i>Tenuitella pseudoedita</i>		12.3	Li et al., 1992
T <i>Tenuitella selleyi</i>		12.3	Li et al., 1992
B <i>Globorotalia fohsi lobata</i>	M9a	12.5	Wright and Miller, 1992
B <i>Globorotalia fohsi s.s.</i>	M8	12.7	Wright and Miller, 1992
B <i>Globorotalia praefohsi</i>		12.7	Wright and Miller, 1992
B <i>Neogloboquadrina nympha</i>		13.4	Berggren, 1992
T <i>Globorotalia peripheroronda</i>		14.6	Berggren et al., 1985
B <i>Globorotalia peripheroacuta</i>	M7	14.8	Berggren et al., 1995a
T <i>Praeorbulina sicana</i>		14.8	Berggren et al., 1985
T <i>Praeorbulina glomerosa s.s.</i>		14.8	Berggren et al., 1985
B <i>Orbulina suturalis</i>	M6	15.1	Berggren et al., 1985
B <i>Orbulina suturalis</i>	(SN6)		Jenkins, 1993
T <i>Globorotalia miozea</i>		15.9	Berggren, 1992
B <i>Praeorbulina circularis</i>		16	Berggren et al., 1985
B <i>Praeorbulina glomerosa</i>	M5b	16.1	Berggren et al., 1995a
B <i>Praeorbulina glomerosa</i>	(SN5)		Jenkins, 1993
B <i>Globigerinoides diminutus</i>		16.1	Berggren et al., 1985
B <i>Praeorbulina curva</i>		16.3	Berggren et al., 1985
B <i>Praeorbulina sicana</i>	M5	16.4	Berggren et al., 1985
T <i>Globorotalia incognita</i>		16.4	Berggren, 1992
B <i>Globorotalia birnageae</i>	M4b	16.7	Berggren et al., 1995a
B <i>Globorotalia miozea</i>		16.7	Berggren, 1992
B <i>Globorotalia birnageae</i>		16.7	Berggren et al., 1985
T <i>Catapsydrax dissimilis</i>	M4	17.3	Berggren et al., 1985
T <i>Globorotalia zealandica</i>		17.3	Li et al., 1992
T <i>Globorotalia semivera</i>		17.3	Berggren et al., 1985
T <i>Globoquadrina dehiscens forma spinosa</i>		17.9	Berggren et al., 1985
B <i>Globorotalia praescitula</i>		18.5	Miller et al., 1994
B <i>Globorotalia insueta</i>	M3	18.8	Berggren et al., 1995a
B <i>Globigerinoides trilobus</i>	(SN4)		Jenkins, 1993
B <i>Globigerinoides altiapertura</i>		20.5	Montanari et al., 1991
B <i>Globoturborotalita connecta</i>	(SN3)	20.9*	Jenkins, 1993; Chaproniere et al., 1995
T <i>Tenuitella munda</i>		21.4	Li et al., 1992
T <i>Globorotalia kugleri</i>	M2	21.5	Montanari et al., 1991
B <i>Globorotalia incognita</i>		21.6	Berggren, 1992
T <i>Globoturborotalita angulisuturalis</i>		21.6	Berggren et al., 1985
T <i>Globorotalia pseudokugleri</i>		21.6	Berggren et al., 1985
B <i>Globoquadrina dehiscens forma spinosa</i>		22.2	Berggren et al., 1985
B <i>Globoturborotalita woodi</i>	(SN2)	22.6*	Jenkins, 1993; Chaproniere et al., 1995
T <i>Globoquadrina globularis</i>		22.8	Berggren et al., 1985
B <i>Globoquadrina dehiscens</i>	M1b	23.2	Berggren et al., 1985
B <i>Globoquadrina dehiscens</i>	(SN1)		Jenkins, 1993; Chaproniere et al., 1995
B <i>Globorotalia kugleri</i>	M1	23.8	Berggren et al., 1985
B <i>Globorotalia mendacis</i>		23.8	Berggren et al., 1985
Oligocene/Miocene boundary		23.8	
T <i>Globigerina euapertura</i>		23.8	Berggren, 1992
T <i>Tenuitella gemma</i>		24.3	Li et al., 1992
FcO <i>Globigerinoides primordius</i>		24.3	Berggren et al., 1985
B <i>Globorotalia pseudokugleri</i>		25.9	Leckie et al., 1993
B <i>Globigerinoides primordius</i>		26.7	Leckie et al., 1993
T <i>Paragloborotalia opima opima</i>	P22	27.1	Berggren et al., 1985
T <i>Globigerina labiacrassata</i>		27.1	Berggren, 1992

Table T2 (continued).

Event	Zone (base)	Age (Ma)	Reference
LcO <i>Chiloguembelina cubensis</i>	P21b	28.5	Li et al., 1992
T <i>Chiloguembelina cubensis</i>	(SP15)		Jenkins, 1993
B <i>Globigerina angulisurealis</i>	P21	28.5	Blow, 1969
B <i>Globigerinita boweni</i>		28.5	Li et al., 1992
B <i>Globigerina angulisurealis</i>	P21a	29.4	Leckie et al., 1993
B <i>Tenuitellinata juvenilis</i>		29.7	Li et al., 1992
T <i>Subbotina angiporoides</i>		30	Berggren, 1992
T <i>Subbotina angiporoides</i>	(SP14)		Jenkins, 1993
T <i>Turborotalia ampliapertura</i>	P20	30.3	Miller et al., 1993
B <i>Paragloborotalia opima opima</i>		30.6	Berggren et al., 1985
T <i>Subbotina brevis</i>	(SP13)	31.5*	Jenkins, 1993; Chaproniere et al., 1995
T <i>Pseudohastigerina</i> spp.	P19	32	Miller et al., 1993
B <i>Subbotina brevis</i>	(SP12)	33.4*	Jenkins, 1993; Chaproniere et al., 1995
B <i>Cassigerinella chipolensis</i>		33.65	Miller et al., 1993
Eocene/Oligocene boundary		33.7	
T <i>Hantkenina</i> spp.		33.7	Coccioni et al., 1988
T <i>Turborotalia cerroazulensis</i>	P18	33.8	Coccioni et al., 1988
T <i>Cribohantkenina inflata</i>	P17	34	Coccioni et al., 1988
T <i>Globigerapsis index</i>		34.3	Berggren, 1992
B <i>Turborotalia cunialensis</i>	P16	35.2	Coccioni et al., 1988
T <i>Turborotalia pomeroli</i>		35.3	PremoliSilva et al., 1988
T <i>Porticulasphaera semiinvoluta</i>		35.3	PremoliSilva et al., 1988
B <i>Cribohantkenina inflata</i>		35.5	Coccioni et al., 1988
T <i>Acarinina</i> spp.		37.50–38.50	Nocchi et al., 1986
T <i>Acarinina aculeata</i>	(SP11)	36.7*	Jenkins, 1993; Chaproniere et al., 1995
T <i>Acarinina collactea</i>		37.7	Berggren et al., 1985
T <i>Subbotina linaperta</i>		37.7	Berggren, 1992
T <i>Morozovella spinulosa</i>		38.1	Berggren et al., 1985
B <i>Porticulasphaera semiinvoluta</i>	P15	38.4	Nocchi et al., 1986
T <i>Planorotalites</i> spp.		38.5	Nocchi et al., 1986
T <i>Acarinina primitiva</i>		39	Stott and Kennett, 1990
T <i>Subbotina frontosa</i>		39.3	Berggren et al., 1985
T <i>Globigerinapsis beckmanni</i>	P14	40.1	Berggren et al., 1986
B <i>Globigerinapsis beckmanni</i>	P13	40.5	Berggren et al., 1987
T <i>Acarinina bullbrookii</i>		40.5	Berggren et al., 1988
B <i>Chiloguembelina cubensis</i>	(SP10)	41.2*	Jenkins, 1993; Chaproniere et al., 1995
B <i>Turborotalia pomeroli</i>		42.4	Berggren et al., 1989
B <i>Globigerapsis index</i>		42.9	Berggren et al., 1990
B <i>Globigerapsis index</i>	(SP9)		Jenkins, 1993
B <i>Morozovella lehneri</i>		43.5	Berggren et al., 1991
T <i>Morozovella aragonensis</i>	P12	43.6	Berggren et al., 1992
B <i>Globigerinapsis kugleri</i>	P11	45.8	Berggren et al., 1995a
B <i>Turborotalia possagnoensis</i>		46	Berggren et al., 1995a
T <i>Morozovella crater</i>	(SP8)	48.8*	Jenkins, 1993; Chaproniere et al., 1995
B <i>Hantkenina nutalli</i>	P10	49	Berggren et al., 1985
B <i>Planorotalites palmerae</i>	P9	50.4	Berggren et al., 1985
T <i>Morozovella formosa</i>	P8	50.8	Berggren, 1969
B <i>Acarinina pentacamerata</i>		50.8	Stott and Kennett, 1990
B <i>Morozovella aragonensis</i>	P7	52.3	Berggren et al., 1995a
T <i>Morozovella marginodentata</i>		52.5	Berggren et al., 1995a
T <i>Morozovella lensiformis</i>		52.7	Berggren et al., 1995a
T <i>Subbotina velascoensis</i>		53.5	Berggren et al., 1995a
T <i>Morozovella aequa</i>		53.6	Berggren et al., 1995a
B <i>M. formosa formosa/M. lensiformis</i>	P6b	54	Berggren and Miller, 1988
B <i>Morozovella crater</i>	(SP7)	54*	Jenkins, 1993; Chaproniere et al., 1995
B <i>Morozovella lensiformis</i>		54	Berggren et al., 1995a
T <i>Morozovella velascoensis</i>	P6	54.7	Berggren et al., 1995a
Paleocene/Eocene boundary		54.7	

Notes: Zone: parentheses = from Jenkins (1993). Age: * = from Chaproniere et al. (1995). B = bottom common occurrence, T = top common occurrence, FcO = first common occurrence, LcO = last common occurrence.

Table T3. Quaternary–Miocene chronostratigraphic units correlated with planktonic foraminifer and calcareous nannofossil zonations and geomagnetic polarity timescale. (See table notes. Continued on next two pages.)

Event	Zone (base)	Age (Ma)	Reference
B acme <i>Emiliana huxleyi</i>		0.085	Blow, 1969
B <i>Emiliana huxleyi</i>	CN15	0.26	Berggren et al., 1995a
T <i>Pseudoemiliana lacunosa</i>	CN14b	0.46	Berggren et al., 1995a
B <i>Gephyrocapsa parallela</i>		0.94	Blow, 1969
Reentrance medium <i>Gephyrocapsa</i> spp.	CN14a?	1.03	Berggren et al., 1995a
T large <i>Gephyrocapsa</i> spp.		1.18	Blow, 1969
B large <i>Gephyrocapsa</i> spp.		1.4	Blow, 1969
T <i>Helicosphaera sellii</i>		1.22	Berggren et al., 1995a
T <i>Calcidiscus macintyreii</i>		1.59	Berggren et al., 1995a
B <i>Gephyrocapsa caribbeanica</i>	CN13b?	1.71	Blow, 1969
Pleistocene/Pliocene boundary		1.8	
T <i>Discoaster brouweri</i>	CN13a	1.95	Blow, 1969
B acme <i>Discoaster triradiatus</i>		2	Blow, 1969
T <i>Discoaster pentaradiatus</i>	CN12d	2.55	Berggren et al., 1995a
T <i>Discoaster surculus</i>	CN12c	2.55	Berggren et al., 1995a
T <i>Discoaster tamalis</i>	CN12b	2.73	Berggren et al., 1995a
T <i>Sphenolithus</i> spp.	CN12a	3.6	Berggren et al., 1995a
T <i>Reticulofenestra pseudumbilicus</i>	CN12a	3.75	Berggren et al., 1995a
T <i>Amaurolithus</i> spp.	CN11	4.5	Blow, 1969
T <i>Ceratolithus acutus</i>		4.57	Berggren et al., 1995a
B <i>Ceratolithus rugosus</i>	CN10c	5.05	Blow, 1969
B <i>Ceratolithus acutus</i>	CN10b	5.09	Blow, 1969
T <i>Triquetrorhabdulus rugosus</i>		5.23	Blow, 1969
Pliocene/Miocene boundary		5.38	
T <i>Discoaster quinquerramus</i>	CN10a	5.6	Berggren et al., 1995a
T <i>Amaurolithus amplifucus</i>		5.9	Berggren et al., 1995a
B <i>Amaurolithus amplifucus</i>		6.6	Berggren et al., 1995a
T paracme <i>Reticulofenestra pseudumbilicus</i>		6.8	Martini, 1971
B <i>Amaurolithus primus</i>	CN9b	7.2	Berggren et al., 1995a
T <i>Discoaster loeblichii</i>		7.4	Berggren et al., 1995a
T <i>Minylitha convalis</i>		7.8	Berggren et al., 1995a
B <i>Discoaster berggrenii</i>	CN9a	8.6	Berggren et al., 1995a
B <i>Discoaster loeblichii</i>		8.7	Berggren et al., 1995a
B paracme <i>Reticulofenestra pseudumbilicus</i>		8.8	Martini, 1971
T <i>Discoaster bollii</i>		9.1	Berggren et al., 1995a
T <i>Catinaster calyculus</i>		9.36	Jenkins, 1985; 1993
T <i>Discoaster hamatus</i>	CN8a	9.4	Berggren et al., 1995a
B <i>Minylitha convallis</i>		9.5	Berggren et al., 1995a
B <i>Discoaster neohamatus</i>		9.6	Martini, 1971
B <i>Discoaster hamatus</i>	CN7	10.7	Berggren et al., 1995a
T <i>Coccolithus miopelagicus</i>		11	Jenkins, 1985; 1993
B <i>Catinaster coalitus</i>	CN6	11.3	Berggren et al., 1995a
T <i>Discoaster kugleri</i>		11.5	Berggren et al., 1995a
B <i>Discoaster kugleri</i>		11.8	Berggren et al., 1995a
T <i>Coronocyclus nitescens</i>		12.1	Martini, 1971
B <i>Calcidiscus macintyreii</i> >11 μ m		12.3	Martini, 1971
B <i>Triquetrorhabdulus rugosus</i>		13.2	Berggren et al., 1995a
T <i>Calcidiscus premacintyreii</i>		12.7	Martini, 1971
T <i>Discoaster signus</i>		12.7	Martini, 1971
Tc <i>Cyclicargolithus floridanus</i>		13.2	Martini, 1971
T <i>Sphenolithus heteromorphus</i>	CN5a	13.6	Berggren et al., 1995a
T <i>Helicosphaera ampliaperta</i>	CN4	15.6	Berggren et al., 1995a
B <i>Discoaster signus</i>		16.2	Martini, 1971
T Abundant <i>Discoaster deflandrei</i>		16.2	Martini, 1971
B <i>Calcidiscus premacintyreii</i>		17.4	Okada and Bukry, 1980
B <i>Sphenolithus heteromorphus</i>	CN3	18.2	Berggren et al., 1995a
T <i>Sphenolithus belemnos</i>		18.3	Berggren et al., 1995a
B <i>Sphenolithus belemnos</i>	CN2	19.2	Berggren et al., 1995a
T <i>Triquetrorhabdulus carinatus</i>		23.1	Berggren et al., 1995a
T <i>Triquetrorhabdulus serratus</i>		23.2	Berggren et al., 1995a
T <i>Sphenolithus umbrellus</i>		23.6	Berggren et al., 1995a
T <i>Sphenolithus capricornutus</i>		23.7	Berggren et al., 1995a
B <i>Discoaster druggi</i>	CN1c	23.3	Berggren et al., 1985a
T <i>Sphenolithus delphix</i>		23.8	Berggren et al., 1995a

Table T3 (continued).

Event	Zone (base)	Age (Ma)	Reference
Miocene/Oligocene boundary		23.8	
T <i>Dictyococcites bisectus</i>	CN1c	23.9	Berggren et al., 1995a
B <i>Sphenolithus delphix</i>		24.3	Berggren et al., 1995a
T <i>Zygrhablithus bijugatus</i>		24.5	Berggren et al., 1995a
T <i>Sphenolithus ciperoensis</i>	CN1a	24.75	Berggren et al., 1995a
T <i>Sphenolithus distentus</i>	CP19b	27.5	Berggren et al., 1995a
T <i>Sphenolithus predistentus</i>		27.5	Berggren et al., 1995a
T <i>Sphenolithus pseudoradians</i>		29.1	Berggren et al., 1995a
B <i>Sphenolithus ciperoensis</i>	CP19a	29.9	Berggren et al., 1995a
B <i>Sphenolithus distentus</i>	CP18	31.5–33.1	Berggren et al., 1995a
T <i>Reticulofenestra umbilicus</i>	CP17	32.3	Berggren et al., 1995a
T <i>Coccolithus formosus</i>	CP16c	32.8	Berggren et al., 1995a
T <i>Chiasmolithus oamaruensis</i>		33.7	Berggren et al., 1995a
Oligocene/Eocene boundary		33.7	
T <i>Discoaster saipanensis</i>	CP16a	34.2	Berggren et al., 1995a
T <i>Discoaster barbadiensis</i>	CP16a	34.3	Berggren et al., 1995a
T <i>Cribo centrum reticulatum</i>		35	Berggren et al., 1995a
B <i>Isthmolithus recurvus</i>		36	Berggren et al., 1995a
T <i>Calcidiscus protoannulus</i>		36.8	Backman, 1987
B <i>Chiasmolithus oamaruensis</i>	CP15	37	Berggren et al., 1995a
T <i>Chiasmolithus grandis</i>	CP15	37.1	Berggren et al., 1995a
B <i>Dictyococcites bisecta</i>		38	Berggren et al., 1995a
T <i>Chiasmolithus solitus</i>	CP14b	40.4	Berggren et al., 1995a
B <i>Dictyococcites hesslandii</i>		41.8	Backman, 1987
T <i>Nannotetrina fulgens</i>		43.1	Berggren et al., 1995a
T <i>Blackites gladius</i>		43.4	Berggren et al., 1995a
B <i>Reticulofenestra umbilicus</i>	CP14a	43.7	Berggren et al., 1995a
T <i>Chiasmolithus gigas</i>	CP13c	44.5	Berggren et al., 1995a
B <i>Chiasmolithus gigas</i>	CP13b	46.1	Berggren et al., 1995a
B <i>Nannotetrina fulgens</i>	CP13a	47.3	Berggren et al., 1995a
T <i>Discoaster lodoensis</i>		47.9	Berggren et al., 1995a
B <i>Rhabdosphaera inflata</i>		48.5	Berggren et al., 1995a
B <i>Nannotetrina</i> spp.		49.2	Backman, 1986
B <i>Discoaster sublodoensis</i>	CP12	49.7	Berggren et al., 1995a
T <i>Tribachiatus orthostylus</i>		50.6	Berggren et al., 1995a
B <i>Discoaster lodoensis</i>	CP10	52.85	Berggren et al., 1995a
T <i>Sphenolithus radians</i>		53.1	Berggren et al., 1995a
T <i>Tribachiatus contortus</i>		53.6	Berggren et al., 1995a
B <i>Tribachiatus orthostylus</i>		53.6	Berggren et al., 1995a
B <i>Discoaster diastypus</i>	CP9a	53.9	Backman, 1986
T <i>Ericsonia robusta</i>		54	Backman, 1986
B <i>Tribachiatus contortus</i>	CP9a	54.3	Berggren et al., 1995a
Eocene/Paleocene boundary			
B <i>Tribachiatus (Rhombaster) bramlettei</i>		55	Backman, 1986
B <i>Rhombaster</i> spp.		55.1	Backman, 1986
T <i>Fasciculithus tympaniformis</i>		55.33	Berggren et al., 1995a
B <i>Camplyosphaera eodela</i>	CP8b	55.5	Berggren et al., 1995a
B <i>Discoaster multiradiatus</i>	CP8a	56.2	Berggren et al., 1995a
B <i>Discoaster okadai</i>		56.8	Berggren et al., 1995a
B <i>Discoaster nobilis</i>	CP7	56.9	Berggren et al., 1995a
B <i>Heliolithus riedelii</i>		57.3	Berggren et al., 1995a
T <i>Heliolithus kleinpellii</i>		56.6	Backman, 1986
B <i>Discoaster mohlerii</i>	CP6	57.5	Berggren et al., 1995a
B <i>Sphenolithus anarrhopus</i>		58.4	Berggren et al., 1995a
T <i>Chiasmolithus danicus</i>		57.5	Berggren et al., 1985a
B <i>Heliolithus kleinpellii</i>	CP5	58.4	Berggren et al., 1995a
B <i>Heliolithus cantabriae</i>		58.2	Backman, 1986
T <i>Fasciculithus pileatus</i>		58.6	Backman, 1986
T <i>Cruciplacolithus tenuis</i>		58.6	Berggren et al., 1985a
B <i>Fasciculithus</i> spp.		59.2	Backman, 1986
B <i>Sphenolithus primus</i>		60.6	Berggren et al., 1995a
B <i>Chiasmolithus bidens</i>		60.7	Berggren et al., 1995a
B <i>Ellipsolithus macellus</i>	CP3	62.2	Berggren et al., 1995a
B <i>Chiasmolithus danicus</i>	CP2	63.8	Berggren et al., 1995a
B <i>Cruciplacolithus tenuis</i>	CP1b	64.5	Berggren et al., 1995a
B <i>Cruciplacolithus primus</i>		64.8	Berggren et al., 1995a
B <i>Biantholithus sparsus</i>		65	Berggren et al., 1995a
T Cretaceous taxa	CP1a	65	Berggren et al., 1995a

Table T3 (continued).

Event	Zone (base)	Age (Ma)	Reference
Tertiary/Cretaceous boundary		65	
B <i>Micula prinsii</i>		66	Erba et al., 1995
B <i>Nephrolithus frequens</i> (low latitude)		67.2	Erba et al., 1995
B <i>Micula murus</i>		68.5	Erba et al., 1995
T <i>Reinhardtites levis</i>		69.4	Erba et al., 1995
T <i>Quadrum trifidum</i>		71.3	Erba et al., 1995
Maastrichtian/Campanian boundary		71.3	
T <i>Tranolithus phacelosus</i>		71.6	Erba et al., 1995
T <i>Aspidolithus parvus</i>		74.6	Erba et al., 1995
T <i>Eiffelithus eximius</i>		75.3	Erba et al., 1995
T <i>Lithastrinus grillii</i>		75.1	Erba et al., 1995
B <i>Quadrum trifidum</i>		76.1	Erba et al., 1995
B <i>Quadrum sissinghii</i>		77.1	Erba et al., 1995
B <i>Ceratolithoides aculeus</i>		78.5	Erba et al., 1995
T <i>Bukryaster hayii</i>		79.8	Erba et al., 1995
T <i>Marthasterites furcatus</i>		80.6	Erba et al., 1995
B <i>Ceratolithoides verbeekii</i>		82	Erba et al., 1995
B <i>Aspidolithus parvus constrictus</i>		83.5	Erba et al., 1995
Campanian/Santonian boundary		83.5	
B <i>Calculites obscurus</i>		83.8	Erba et al., 1995
B <i>Lucianorhabdus cayeuxii</i>		84.8	Erba et al., 1995
T <i>Lithastrinus septenarius</i>		84.9	Erba et al., 1995
B <i>Lithastrinus grillii</i>		85.8	Erba et al., 1995
Santonian/Coniacian boundary		85.8	
B <i>Reinhardtites anthophorus</i>		85.8	Erba et al., 1995
B <i>Micula decussata</i>		87.2	Erba et al., 1995
Coniacian/Turonian boundary		89	
B <i>Marthasterites furcatus</i>		89.3	Erba et al., 1995
B <i>Lucianorhabdus maleformis</i>		91	Erba et al., 1995
B <i>Eiffelithus eximius</i>		91	Erba et al., 1995
Turonian/Cenomanian boundary		93.5	
T <i>Corollithion kennedyi</i>		93.9	Erba et al., 1995
T <i>Rhagodiscus asper</i>		93.9	Erba et al., 1995
T <i>Axopodorhabdus albianus</i>		93.9	Erba et al., 1995
T <i>Microstaurus chiastius</i>		94.4	Erba et al., 1995
B <i>Microrhabdulus decoratus</i>		95.2	Erba et al., 1995
B <i>Lithraphidites acutus</i>		95.2	Erba et al., 1995
B <i>Corollithion kennedyi</i>		97.4	Erba et al., 1995
Cenomanian/Albian boundary		98.9	
T <i>Hayesites albiensis</i>		99	Erba et al., 1995
T <i>Rucinolithus irregularis</i>		99	Erba et al., 1995
B <i>Eiffelithus turriseiffelii</i>		101.7	Erba et al., 1995
B small <i>Eiffelithus</i> spp.		103.8	Erba et al., 1995
B <i>Axopodorhabdus albianus</i>		106.5	Erba et al., 1995
B <i>Tranolithus phacelosus</i>		106.5	Erba et al., 1995
B <i>Cribrosphaerella ehrenbergii</i> sensu Erba		110.3	Erba et al., 1995
Albian/Aptian boundary		112.2	
B <i>Prediscosphaera columnata</i> <5 µm		112.5	Erba et al., 1995
T <i>Assipetra intracretacea</i>		113	Erba et al., 1995
B <i>Hayesites albiensis</i>		114	Erba et al., 1995
T <i>Micrantholithus hoschulzii</i>		114.2	Erba et al., 1995
T <i>Nannoconus</i> st. <i>steinmanii</i>		114.2	Erba et al., 1995
B <i>Braarudosphaera africana</i>		118.2	Erba et al., 1995
B <i>Stoverius achylosum</i>		118.2	Erba et al., 1995
B <i>Eprolithus floralis</i>		119	Erba et al., 1995
B <i>Rhagodiscus angustus</i>		119.9	Erba et al., 1995
T <i>Nannoconid</i> paracme		120.5	Erba et al., 1995
Aptian/Barremian boundary		121	
B <i>Rucinolithus irregularis</i>		121.1	Erba et al., 1995
B <i>Flabellites oblongus</i>		121.1	Erba et al., 1995

Notes: Timescales in Age column are from Berggren et al. (1995a). B = bottom of common occurrence, T = top of common occurrence, Tc = top common.

**Table T4.** Compilation of types and storage treatments for samples taken during microbiological sampling, Sites U1316, U1317, and U1318.

Code	Sample type (cm)		Sample	Storage treatment	Sites sampled		
	WRC	Syringe			U1316	U1317	U1318
HS		5	Methane headspace	Processed on ship	X	X	X
CH4		5	Detailed methane	Gas vial	X	X	X
DEL		5	$\delta^{13}\text{C}$ -methane	Gas vial	X	X	X
HGA		5	Higher hydrocarbon analyses	Gas vial	X	X	X
IW	10–20		Interstitial water	Processed on ship	X	X	X
CONT-PFT		5	PFT contamination tests	Gas vial	X	X	X
CONT-BEAD		5	Bead contamination tests	Gas vial	X	X	X
AODC		5	Direct bacterial counts	Fomaldehyde	X	X	X
AOM	30		Rates of anaerobic oxidation of methane	In nitrogen +4°C, anoxic	X	X	X
SRR	10		Rates of sulfate reduction, dehalogenation experiments	In nitrogen +4°C, anoxic	X	X	X
CH4C	20		Rates of methanogenesis and thymidine incorporation, MPN enrichments	In nitrogen +4°C, anoxic	X	X	X
URI	5		Rates of hydrogenase activity	In nitrogen –80°C, anoxic	X	X	X
GAS	6		Methane isotopes and higher hydrocarbon gas concentrations	+4°C poisoned (NaN_3)	X	X	X
VIR	5		Viren	In nitrogen –80°C, anoxic	X	X	X
FISH	5		CARD-FISH	In nitrogen –80°C, anoxic	X	X	X
DNAI	5		DNA-qPCR Div	–80°C	X	X	X
DNAPCR	5		qPCR quantification of bacterial and archaeal populations	–80°C	X	X	X
DNAS	5		DNA plasmid vectors	–80°C		X	X
DNAG	5		CARD-FISH and 16S rRNA analysis of AOM communities	–80°C	X	X	X
DNAIODP	5		IODP DNA archive core	–80°C	X	X	X
AALEO	5		Amino acids	–80°C	X	X	X
DNAC	10		DNA extraction, amplification, DGGE, functional genes <i>dsrAB</i> and <i>mcrA</i>	–80°C	X	X	X
LIPH	5		Intact phospholipids	–80°C	X	X	X
WRCB	30		Oedometry	Room temperature	X		X
LIPD	5		Archaeal tetra-ether membrane lipids	–80°C		X	
MICT	5		Microtomography	Room temperature		X	

Notes: PFT = perfluorocarbon tracer. MPN = most probable number, CARD-FISH = catalyzed reporter deposition–fluorescent in situ hybridization. IODP = Integrated Ocean Drilling Program. DNA = deoxyribonucleic acid. WRC = whole-round core. qPCR = quantitative polymerase chain reaction, rRNA = ribosomal ribonucleic acid, AOM = anaerobic oxidation of methane, DGGE = denaturing gradient gel electrophoresis, *dsrAB* = dissimilatory sulfite reductase, *mcrA* = methyl-coenzyme M reductase.

Table T5. Summary of sampling intervals for all physical properties measurements made during Expedition 307.

Measurement	Tool abbreviation	Sampling interval	Comments
Magnetic susceptibility (MS)	MSCL	5 cm	5 times at 1 s period
Wet bulk density (GRA)	MST	5 cm	5 times at 1 s period
Compressional wave velocity (PWL)	MST	5 cm	5 times at 1 s period
Magnetic susceptibility (MS)	MST	5 cm	5 times at 1 s period
Natural gamma radiation (NGR)	MST	5 cm	5 times at 1 s period
Thermal conductivity	ThermCon	One per core	Only measured in unconsolidated sediment middle of the section
Undrained shear strength		Three per section	At 30, 80, 130 cm
Dry and wet bulk density	MAD	Two per section	At 25, 100 cm
P-wave velocity (x-direction)	PWS3	Three per section	At 30, 80, 130 cm

Table T6. Measurements and specifications for wireline logging tools.

Tool string*	Tool	Measurement	Sampling interval (cm)	Approximate vertical resolution (cm)
Triple combination	HNGS	Spectral gamma ray	15	51
	APS	Porosity	5 and 15	43
	HLDS	Bulk density	2.5	38
	EMS	Environmental (mud temperature and resistivity)	15	NA
	DIT-E	Resistivity	15	200/150/76
	TAP	Temperature	1 per s	NA
		Tool acceleration	4 per s	NA
Pressure		1 per s	NA	
Formation MicroScanner (FMS)-sonic combination	SGT	Total gamma ray	15	46
	DSI	Acoustic velocity	15	107
	GPIT	Tool orientation	0.25 and 15	NA
	FMS	Microresistivity	0.25	0.5
Well Seismic Tool (WST-3 components) stationary measurements	WST-3	Sonic traveltime	Variable	NA

Notes: * = all tool and tool string names (except the TAP tool) are trademarks of Schlumberger. For additional information about tool physics and use, consult IODP-USIO Science Services, LDEO, at iodp.ldeo.columbia.edu/TOOLS_LABS/tools.html. See Table T7 for explanations of acronyms used to describe tool strings and tools. NA = not applicable.

Table T7. Acronyms and units used for wireline logging tools.

Tool	Output	Tool name/Explanation of output	Unit
APS		Accelerator Porosity Sonde	
	APLC	Near array porosity (limestone calibrated)	%
	SIGF	Formation capture cross section (S_f)	Capture units
	STOF	Tool standoff (computed distance from borehole wall)	inches
DIT-E		Dual Induction Tool	
	IDPH	Deep induction resistivity	Ω -m
	IMPH	Medium induction resistivity	Ω -m
	SFLU	Spherically focused resistivity	Ω -m
DSI		Dipole Sonic Imager	
	DTCO	Compressional wave delay time (Dt)	ms/ft
	DTSM	Shear wave delay time (Dt)	ms/ft
	DTST	Stoneley wave delay time (Dt)	ms/ft
FMS		Formation MicroScanner	
	C1, C2	Orthogonal hole diameters	inches
	P1AZ	Pad 1 azimuth Spatially oriented resistivity images of borehole wall	Degrees
GPIT		General Purpose Inclinator Tool	
	DEVI	Hole deviation	Degrees
	HAZI	Hole azimuth	Degrees
	F_x, F_y, F_z A_x, A_y, A_z	Earth's magnetic field (three orthogonal components) Acceleration (three orthogonal components)	Degrees m/s^2
HLDS		Hostile Environment Litho-Density Sonde	
	RHOM	Bulk density	g/cm^3
	PEFL	Photoelectric effect	b/e ⁻
	LCAL	Caliper (measure of borehole diameter)	inches
	DRH	Bulk density correction	g/cm^3
HNGS		Hostile Environment Gamma Ray Sonde	
	HSGR	Standard (total) gamma ray	gAPI
	HCGR	Computed gamma ray (HSGR minus uranium contribution)	gAPI
	HFK	Potassium (K)	wt%
	HTHO	Thorium (Th)	ppm
	HURA	Uranium (U)	ppm
EMS		Environmental Measurement Sonde	
	TMP	Temperature	$^{\circ}C$
SGT		Scintillation Gamma Ray Tool	
	ECGR	Environmentally corrected gamma ray	gAPI
TAP		Temperature/Acceleration/Pressure tool	$^{\circ}C, m/s^2, psi$
WST		Well Seismic Tool (1 component) Acoustic arrival times	ms

Notes: * = all tool and tool string names (except the TAP tool) are trademarks of Schlumberger. For the complete list of acronyms used in IODP and for additional information about tool physics and use, consult IODP-USIO Science Services, LDEO, at iodp.ldeo.columbia.edu/TOOLS_LABS/tools.html.